Widespread and Persistent Ozone Pollution in Eastern China during the Non-winter Season of 2015: Observations and Source Attributions

Guohui Li[1*], Naifang Bei[2], Junji Cao[1*], Jiarui Wu[1], Xin Long[1], Tian Feng[1, 2], Wenting Dai[1], Suixin Liu[1], Qiang Zhang[3], and Xuexi Tie[1]

[1]Key Lab of Aerosol Chemistry and Physics, SKLLQG, Institute of Earth Environment, Chinese Academy of Sciences, Xi'an, China
[2]School of Human Settlements and Civil Engineering, Xi'an Jiaotong University, Xi'an, Shaanxi, China
[3]Department of Environmental Sciences and Engineering, Tsinghua University, Beijing, China
[*]Correspondence to: Guohui Li (ligh@ieecas.cn) and Junji Cao (jjcao@ieecas.cn)

Abstract: Rapid growth of industrialization, transportation, and urbanization has caused increasing emissions of ozone (O_3) precursors recently, enhancing the O_3 formation in Eastern China. We show here that Eastern China has experienced widespread and persistent O_3 pollution from April to September in 2015 based on the O_3 observations in 223 cities. The observed maximum 1-h O_3 concentrations exceed 200 μg m^{-3} in almost all the cities, 400 μg m^{-3} in more than 25% of the cities, and even 800 μg m^{-3} in six cities in Eastern China. The average daily maximum 1-h O_3 concentrations are more than 160 μg m^{-3} in 45% of the cities, and the 1-h O_3 concentrations of 200 μg m^{-3} have been exceeded on over 10% of days from April to September in 129 cities. Analyses of pollutants observations from 2013 to 2015 have shown that the concentrations of CO, SO_2, NO_2, and $PM_{2.5}$ from April to September in Eastern China have considerably decreased, but the O_3 concentrations have increased by 9.9%. A widespread and severe O_3 pollution episode from 22 to 28 May 2015 in Eastern China has been simulated using the WRF-CHEM model to evaluate the O_3 contribution of biogenic and various anthropogenic sources. The model generally performs reasonably well in simulating the temporal variations and spatial distributions of near-surface O_3 concentrations. Using the factor separate approach, sensitivity studies have indicated that the industry source plays the most important role in the O_3 formation, and constitutes the culprit of the severe O_3 pollution in Eastern China. The transportation source contributes considerably to the O_3 formation, and the O_3 contribution of the residential source is not significant generally. The biogenic source provides a background O_3 source, and also plays an important role in the south of Eastern China. Further model studies are needed to comprehensively investigate O_3 formation for supporting the design and implementation of O_3 control strategies, considering rapid changes of emissions inventories and photolysis caused by the 'Atmospheric Pollution Prevention and Control Action Plan', released by the Chinese State Council in 2013.

1 Introduction

In the urban planetary boundary layer (PBL), ozone (O_3) is formed as a result of photochemical reactions involving volatile organic compounds (VOCs) and nitrogen oxide (NO_x) in the presence of sunlight (Brasseur et al., 1999):

$$NO_2 + h\nu \rightarrow NO + O(^3P) \quad (290\,nm < \lambda < 420\,nm)$$

$$O(^3P) + O_2 + M \rightarrow O_3 + \mathrm{M}$$

$$O_3 + h\nu \rightarrow O_2 + O(^1D) \quad (290\,nm < \lambda < 329nm)$$

$$O(^1D) + H_2O \rightarrow 2OH$$

$$OH + VOCs + O_2 \rightarrow RO_2 + others$$

$$RO_2 + NO \rightarrow RO + NO_2$$

where $h\nu$ represents the energy of a photon; $O(^3P)$ and $O(^1D)$ represent the ground state and electronically excited oxygen atoms, respectively; RO_2, RO, and OH denote peroxy, oxy, and hydroxyl radicals, respectively. High O_3 concentrations ([O_3]) are of major environmental concerns due to its deleterious impacts on ecosystems (e.g., National Research Council, 1991) and human health (Lippman, 1993; Weinhold, 2008).

The emissions of O_3 precursors, VOCs and NO_x, have been significantly increased recently in China due to rapid industrialization and urbanization, and increasing transportation activity (e.g., Zhang et al., 2009; Kurokawa et al., 2013; Yang et al., 2015). Satellite measurements have demonstrated that NO_x emissions have been increased by a factor of 2 in Central and East China from 2000 to 2006 (Richter et al., 2005). Zhang et al. (2009) have also shown an increasing trend of NO_x emissions with an enhancement of 55% in China from 2001 to 2006. NO_x emissions have still continued to increase since 2006, caused by increasing power plants and vehicles (Wang et al., 2012; Wang et al., 2013; Yang et al., 2015). In addition, the agriculture has been proposed to have a large potential to produce NO_x (Oikawa et al., 2015). VOCs emissions have been estimated to increase by 29%

during 2001 – 2006 in China (Zhang et al., 2009), and predicted to increase by 49% by 2020 relative to 2005 levels (Xing et al., 2011). Additionally, modeling studies have been performed to investigate the O_3 pollution in Eastern China (Wang et al., 2010; Liu et al., 2012; Situ et al., 2013; Huang et al., 2015). For example, Tie et al. (2013) have analyzed the characteristics of regional O_3 formation to explain the O_3 pollution in Shanghai and its surrounding area using the WRF-CHEM model. Using the observation-based chemical model, Xue et al. (2014) have provided insights into the ozone pollution in Beijing, Shanghai, and Guangzhou by analyzing the O_3 precursors and the potential impacts of heterogeneous chemistry.

Increasing O_3 precursors emissions has caused O_3 to be one of the most serious air pollutants of concern during summertime, particularly in Eastern China, including the North China Plain (NCP), Yangtze River Delta (YRD), and Pearl River Delta (PRD) (e.g., Xu et al., 2011; Tie et al., 2013; Li et al., 2013; Feng et al., 2016). For example, a maximum O_3 concentration of 286 ppb has been observed in urban plumes from Beijing (Wang et al., 2006). Chen et al. (2015) have reported that the average maximum daily [O_3] exceed 150 μg m^{-3} in the summer of 2015 at most of monitoring sites in Beijing. Wu et al. (2016) have also shown that, during summertime of 2015 in Beijing, the average O_3 concentration in the afternoon is 163.2 μg m^{-3}, and the frequency of the O_3 exceedance with hourly [O_3] exceeding 200 μg m^{-3} is 31.8%. In addition, Cheng et al. (2016) have demonstrated an increasing trend of daily maximum 1-h [O_3] from 2004 to 2015 in Beijing, and Ma et al. (2016) have reported significant increase of surface O_3 at a rural site in NCP. In PRD region, the annual average near-surface O_3 level has been reported to increase from 24 ppbv in 2006 to 29 ppbv in 2009, and the maximum 1-h [O_3] can be up to 150 ~ 200 ppb in the summer and fall (Ou et al., 2016, EST). Numerous studies have been performed to examine the severe O_3 pollution in China, but primarily confined to mega-cities or industrial complexes. Few

91 studies have been conducted in whole Eastern China to investigate the O_3 pollution situation
92 and formation.
93 The China's Ministry of Environmental Protection (China MEP) has commenced to
94 release real-time hourly observations of pollutants, including O_3, NO_2, CO, SO_2, $PM_{2.5}$, and
95 PM_{10} (particulate matter with aerodynamic diameter less than 2.5 and 10 μm, respectively)
96 since 2013. In Eastern China, there are 65 cities with air pollutants observations in 2013
97 during summertime, mainly concentrated in Beijing-Tianjin-Hebei (BTH), YRD, and PRD
98 (Figure 1). In 2015, a total of 223 cities have air pollutants observation in Eastern China,
99 providing a good opportunity to explore the O_3 pollution distributions. Therefore, in the
100 present study, the O_3 pollution situation in 2015 is first analyzed from April to September
101 when [O_3] are high in Eastern China. A high O_3 episode occurred in Eastern China in 2015 is
102 simulated using the WRF-CHEM model to evaluate the O_3 formation from biogenic and
103 various anthropogenic sources. The WRF-CHEM model configuration and methodology are
104 described in Section 2. Data analysis and model results are presented in Section 3, and
105 conclusions and discussions are given in Section 4.
106
107 **2 Model and Methodology**
108 **2.1 WRF-CHEM Model and Configurations**
109 In the present study, we use a specific version of the WRF-CHEM model (Grell et al.,
110 2005) to investigate the O_3 formation in Eastern China. The model is developed by Li et al.
111 (2010; 2011a, b; 2012) at the Molina Center for Energy and the Environment, including a
112 new flexible gas phase chemical module and the CMAQ/Models3 aerosol module developed
113 by US EPA (Binkowski and Roselle, 2003). The wet deposition of chemical species is
114 calculated using the method in the CMAQ module and the dry deposition parameterization
115 follows Wesely (1989). The FTUV is used to calculate photolysis rates (Tie et al., 2003; Li et

al., 2005), considering the impacts of aerosols and clouds on the photochemistry (Li et al., 2011b). The ISORROPIA Version 1.7 is used to calculate the inorganic aerosols (Nenes et al., 1998). The secondary organic aerosol (SOA) is predicted using a non-traditional SOA module, including the volatility basis-set (VBS) modeling approach and SOA contributions from glyoxal and methylglyoxal. Detailed information about the WRF-CHEM model can be found in Li et al. (2010; 2011a, b; 2012).

A high O_3 pollution episode from 22 to 28 May 2015 in Eastern China is simulated using the WRF-CHEM model. The WRF-CHEM model adopts one grid with horizontal resolution of 10 km and 35 sigma levels in the vertical direction, and the grid cells used for the domain are 350 × 350 (Figure 1). The physical parameterizations include the microphysics scheme of Hong et al (Hong and Lim, 2006), the Mellor, Yamada, and Janjic (MYJ) turbulent kinetic energy (TKE) planetary boundary layer scheme (Janjić, 2002), the Unified Noah land-surface model (Chen and Dudhia, 2001), the Goddard long wave (Chou and Suarex, 2001) and shortwave parameterization (Chou and Suarex, 1999). The NCEP 1° × 1° reanalysis data are used to obtain the meteorological initial and boundary conditions, and the meteorological simulations are not nudged in the study. The chemical initial and boundary conditions are interpolated from the 6h output of MOZART (Horowitz et al., 2003). The spin-up time of the WRF-CHEM model is 28 hours, which is generally long enough for simulations considering that the initial and boundary conditions are adopted from MOZART, a global chemical transport model. The SAPRC-99 chemical mechanism is used in the present study. The anthropogenic emissions are developed by Zhang et al. (2009), including contributions from agriculture, industry, power generation, residential, and transportation sources. The biogenic emissions are calculated online using the MEGAN (Model of Emissions of Gases and Aerosol from Nature) model developed by Guenther et al (2006). Detailed model configurations are given in Table 1. The simulation domain is shown in

Figure 1.

For discussion convenience, Eastern China is divided into four sections: 1) the Northeast China (including Heilongjiang, Jilin, Liaoning, and the east part of Inner Mongolia, hereafter referred to as NEC), 2) the North China Plain and surrounding areas (including Beijing, Tianjin, Hebei, Shandong, Henan, Shanxi, and the north part of Jiangsu and Anhui, hereafter referred to as NCPs), 3) the YRD and surrounding areas (including the south part of Jiangsu and Anhui, Shanghai, Zhejiang, and Hubei, hereafter referred to as YRDs), and 4) the PRD and surrounding areas (including Fujian, Jiangxi, Hunan, Guangxi, and Guangdong, hereafter referred to as PRDs) (shown in Supplementary Information (SI), SI-Figure 1).

2.2 Statistical Methods for Comparisons

We use the mean bias (*MB*) and the index of agreement (*IOA*) to assess the WRF-CHEM model performance in simulating air pollutants against measurements.

$$MB = \frac{1}{N}\sum_{i=1}^{N}(P_i - O_i)$$

$$IOA = 1 - \frac{\sum_{i=1}^{N}(P_i - O_i)^2}{\sum_{i=1}^{N}(|P_i - \bar{O}| + |O_i - \bar{O}|)^2}$$

where P_i and O_i are the calculated and observed pollutant concentrations, respectively. N is the total number of the predictions used for comparisons, and $\bar{O}$ represents the average of the prediction and observation, respectively. The *IOA* ranges from 0 to 1, with 1 showing perfect agreement of the prediction with the observation.

2.3 Air Pollutants Measurements

The hourly near-surface CO, NO_2, SO_2, and $PM_{2.5}$ mass concentrations from April to September 2015 in Eastern China are released by China MEP, and can be downloaded from the website http://www.aqistudy.cn/. China MEP releases the pollutants observations using the mass concentration (μg m^{-3} or mg m^{-3}) as the unit. Therefore, in order to keep consistent with the observations, the mass concentration is used in the manuscript, although the mixing ratio (such as ppbv) is a more common unit used in the literature for air pollutants.

3 Results and Discussions

3.1 O_3 pollution in Eastern China

Continuous deterioration of air qualtiy in China has engendered the implementation of "Atmospheric Pollution Prevention and Control Action Plan" (hereafter referred to as APPCAP), released by Chinese State Council in September 2013 to reduce $PM_{2.5}$ by up to 25% by 2017 relative to 2012 levels. Therefore, variations of air pollutants from 2013 to 2015 demonstrate the mitigation effects of implementation of the APPCAP on the air quality to a considerable degree. A total of 65 cities, with 427 monitoring sites, have air pollutants observations from 2013 to 2015 during April to September in Eastern China (Figure 1). Considering the occurrence of high [O_3] in the afternoon (12:00 – 18:00 Beijing Time (BJT)), Table 2 provides the average concentrations of air pollutants in the afternoon from April to September in the 65 cites of Eastern China in 2013 and 2015. Apparently, implementation of the APPCAP has decreased the mass concentrations of CO, SO_2, NO_2, and $PM_{2.5}$ in Eastern China, particularly with regard to SO_2, with a reduction of close to 40% from 2013 to 2015. The [O_3] however exhibit an increasing trend, enhanced by 9.9% from 2013 to 2015. Additionally, if the O_3 exceedance is defined as hourly [O_3] exceeding 200 μg m^{-3} (the second grade of National Ambient Air Quality Standards in China), the O_3 exceedance frequency in the afternoon has increased from 5.2% in 2013 to 6.8% in 2015, enhanced by about 31.5%. The ozone monitoring instrument (OMI) satellite observations have also shown that the annual O_3 concentration has increased by 1.6% per year over central and eastern China from 2005 to 2014 (Shan et al., 2016).

There are several possible reasons for the O_3 pollution deterioration in Eastern China since implementation of the APPCAP. Firstly, if the O_3 production regime in Eastern China is VOC-sensitive, the decrease of NO_x due to implementation of the APPCAP likely

191 enhances the O_3 formation. Secondly, mitigation of $PM_{2.5}$ or aerosols directly or indirectly
192 increases the photolysis rates and expedites the O_3 formation. Thirdly, increasing
193 transportation activities enhances the emissions of VOCs and semi-VOCs, facilitating the O_3
194 formation. In addition, variability of meteorological situations also leads to the [O_3]
195 fluctuation (Calkins et al., 2016). Hence, implementation of the APPCAP does not help
196 mitigate [O_3], and unfortunately, severe O_3 pollutions have been looming in Eastern China.
197 In 2015, O_3 observations have been performed in 223 cities with 1064 monitoring sites
198 in Eastern China, which are used to analyze the O_3 pollution situation from April to
199 September. For comparisons, Figure 2 shows the distribution of observed maximum 1-h [O_3]
200 in Mainland China from April to September in 2015. The cities with the maximum 1-h [O_3]
201 exceeding 300 μg m^{-3} are mainly concentrated in NCPs, YRDs, and PRD. In Eastern China,
202 there are only two cities with the maximum 1-h [O_3] less than 200 μg m^{-3}. About 28% of
203 cities have observed more than 400 μg m^{-3} [O_3] (about 200 ppb), showing widespread O_3
204 pollution in Eastern China. Furthermore, it is worth to note that the observed maximum 1-h
205 [O_3] in six cites exceed 800 μg m^{-3} (about 400 ppb), in a very dangerous level.
206 Figure 3 presents the distribution of average daily maximum 1-h [O_3] in Mainland
207 China from April to September 2015. The average daily maximum 1-h [O_3] are more than
208 120 μg m^{-3} in more than 95% of the cities, and 160 μg m^{-3} in 46% of the cities in Eastern
209 China. Particularly, there are seven cities with the average daily maximum 1-h [O_3]
210 exceeding 200 μg m^{-3} during six months. Figure 4 and 5 show the distributions of exceedance
211 days with the maximum 1-h [O_3] exceeding 160 and 200 μg m^{-3} in Mainland China from
212 April to September 2015, respectively. There are more than 60 days with the maximum 1-h
213 [O_3] exceeding 160 μg m^{-3} in 114 cities, and even more than 90 days in 62 cites in Eastern
214 China from April to September. The 1-h [O_3] of 200 μg m^{-3} have been exceeded on over 10%

of days in 129 cities, and on 30% of days in 38 cities (Figure 5). Hence, persistent O_3 pollution has occurred in Eastern China from April to September in 2015.

Furthermore, in the urban PBL, high [O_3] generally take place under calm or stable circumstances with strong solar radiation. From April to September, the East Asian summer monsoon influences Eastern China, causing intensified precipitation which inhibits the high O_3 formation through washing out O_3 precursors and decreasing photolysis rates. So if excluding rainy days in the analysis, the O_3 pollution becomes more severe in Eastern China. For example, in Beijing, there are 54 rainy days and 65 days with the maximum 1-h [O_3] exceeding 200 μg m^{-3} from May to August in 2015. If it does not rain in Beijing, the occurrence possibility of the maximum 1-h [O_3] exceeding 200 μg m^{-3} is around 94%, showing severe and persistent O_3 pollution.

3.2 Model Performance

The hourly measurements of O_3 and NO_2 in Eastern China are used to validate the WRF-CHEM model simulations. Figure 6 presents the distributions of calculated and observed near-surface [O_3] along with the simulated wind fields at 15:00 BJT from 22 to 27 May 2015. In order to interpret the effect of meteorological and synoptic conditions on the air quality in Eastern China, SI-Figure 2 presents the average geopotential height wind filed at 500 hPa from 22 to 27 May 2015. During the study episode, the NCPs and NEC are generally located behind the trough whose center is located between 120°E and 130°E. At the end of May, the main part of subtropical high at 500 hPa locates at the western Pacific, with the ridgeline moving around the 10°N -15°N. With the onset of summer monsoon, the subtropical high gradually moves northwards and affects Southern China, with more precipitation occurrence over YRDs and PRDs. Figure 6 presents the distributions of calculated and observed near-surface [O_3] along with the simulated wind fields at 15:00 BJT from 22 to 27 May 2015. On May 22, Eastern China is influenced by the high-pressure

whose center locates over the Yellow sea, which is induced by the high level trough. The east winds in the south of the high transport humid air into PRDs, causing rainfall weather that substantially decreases [O_3]. The WRF-CHEM model well reproduces the observed low [O_3] in the south of PRDs. In NCPs and YRDs, calm winds, clear sky, and high temperature, induced by the high, facilitate the O_3 formation, and the simulated [O_3] generally exceed 160 μg m^{-3}, which is consistent with the observations. On May 23, the subtropical high moves northward, also causing the rainfall belt in the south of PRDs to extend northward. The simulated O_3 pollution in NCPs is deteriorated and also extended to NEC, in good agreement with the measurements. From May 24 to 25, the high pressure located at the Yellow sea continuously deteriorates the O_3 pollution in Eastern China. The simulated and observed O_3 pollution on May 25 is widespread almost in Eastern China, and the Northwest China also experiences high O_3 pollution. On May 26 and 27, the simulated and observed [O_3] in the north of NCPs and NEC are still high, but in PRDs and YRDs, the [O_3] have been significantly decreased due to the precipitation caused by the subtropical high and summer monsoon.

Generally, the simulated O_3 spatial patterns are consistent with observations, but the model underestimation or overestimation still exists. For example, the model remarkably overestimates the observed [O_3] on May 24, and also cannot well reproduce the high [O_3] on May 25 in PRD. There are several reasons for the model biases in simulating [O_3] distribution. Firstly, the meteorological situations play a key role in air pollution simulations (Bei et al., 2010, 2012), determining the formation, transformation, diffusion, transport, and removal of the air pollutants. Therefore uncertainties in meteorological fields simulations significantly influence the air pollutants simulations. On May 24, the model fails to predict the rainy or overcast weather, leading to remarked overestimation of [O_3] in PRD. Secondly, the 10 km horizontal resolution is used in simulations, which cannot resolve well cumulus

clouds. The model overestimates the [O_3] observed in some cities with [O_3] much lower than their surrounding cities, which is primarily caused by the model failure in resolving convections. Thirdly, the fast changes in emissions are not reflected in the emissions inventories used in the present study.

Figure 7 provides the diurnal profiles of calculated and observed near-surface [O_3] averaged over the ambient monitoring sites in provinces and municipalities in Eastern China during the episode. The model reasonably well reproduces the temporal variations of surface [O_3] compared to observations, e.g., peak [O_3] in the afternoon due to active photochemistry and low [O_3] during nighttime caused by the NO_x titration. Three provinces in NEC, Jilin, Liaoning, and Inner Mongolia, are apparently impacted by the trans-boundary transport from NCPs when the south winds are prevailing (Figure 6). So the uncertainties of wind field simulations constitute one of the most important reasons for the model biases in modeling [O_3] in these three provinces. The model underestimates considerably the observed [O_3] in the three provinces (Figures 7a, c, d), with *MB*s exceeding 19 μg m^{-3}. The model generally exhibits good performance in simulating [O_3] variations in the provinces of NCPs (Figures 7e-l) with *IOA*s exceeding 0.90, but is subject to underestimate the observations, particularly in Beijing which is also significantly influenced by the trans-boundary transport (Wu et al., 2016). In YRDs, the model cannot well predict the observed [O_3] in Shanghai, which is affected by the sea breeze when the large-scale wind fields are weak. In general, however, current numerical weather prediction models, even in research mode, still have difficulties in producing the location, timing, depth, and intensity of the sea-breeze front (Banta et al., 2005; Wang et al., 2013). The model reasonably predicts the [O_3] variations compared to measurements in PRDs (Figures 7p-t) with *IOA*s more than 0.7, but overestimates the observed [O_3] with *MB*s varying from 3.8 to 16.7 μg m^{-3}, showing model biases in modeling precipitation processes.

The comparisons of simulated vs. observed distributions and temporal variations of NO_2 mass concentrations ([NO_2]) are shown in Supplementary Information (SI, SI-Figures 3 and 4). The simulated high near-surface [NO_2] are mainly concentrated in NCP, YRD, and PRD, which is generally consistent with the measurements. The model also reasonably yields temporal variations of [NO_2] compared to measurements, but the simulations of [NO_2] are not as good as those of [O_3], and the *IOA*s in Liaoning, Tianjin, and Shanghai are lower than 0.5. The difference between simulations and observations are frequently rather large during nighttime, which perhaps caused by the model biases in modeling nighttime PBL or the complexity of nighttime chemistry. Another possible reason for NO_x biases in simulations is lack of consideration of the NO_x emissions in the agricultural region, which has been proposed to generate high NO_x emissions under high-temperature conditions (Oikawa et al., 2015). In general, the calculated distributions and variations of [O_3] and [NO_2] are consistent with the corresponding observations, showing that the simulations of meteorological fields and emissions inventories are reasonable, providing the base for sensitivity studies.

3.3 Sensitivity Studies

O_3 formation in the PBL is a complicated nonlinear process, depending on its precursors of NO_x and VOCs from biogenic and various anthropogenic sources. It is imperative to evaluate the O_3 contribution from various sources for devising the O_3 control strategy. Rapid growth of industries, transportation, and urbanization has caused increasing emissions of NO_x and VOCs in Eastern China (e.g., Zhang et al., 2009; Huang et al., 2011; Wang et al., 2012; Wang et al., 2013; Yang et al., 2015). Numerous studies have also demonstrated that biogenic VOCs, such as isoprene and monoterpenes, play a considerable role in the O_3 formation in the PBL (e.g., Chameides et al., 1988; Tao et al., 2003; Li et al., 2007; 2014). Therefore, sensitivity studies are used to evaluate the O_3 contributions of biogenic, industry, residential, and transportation sources in Eastern China, respectively. It is

315 worth to note that emissions of power plants are directly associated with residential living
316 and industrial activities. So in the study, 75% of emissions from power plants are assigned to
317 the industry source and the rest are assigned to the residential source according to the ratio of
318 the power consumption used in industrial activities to residential living (Wang et al., 2016).
319 The factor separation approach (FSA) is used to evaluate the contribution of some
320 emission source to the O_3 concentration by differentiating two model simulations: one with
321 all emissions sources and the other without some emission source. Therefore, except the
322 control simulations with all emissions, additional four sensitivity simulations are performed,
323 in which the biogenic, industry, residential, and transportation emissions are excluded,
324 respectively, to assess their corresponding contributions to the O_3 formation in Eastern China.
325 Figure 8 shows the contribution of near-surface [O_3] averaged in the afternoon during
326 the whole episode from industry, residential, transportation, and biogenic emissions. The
327 industry source plays a more important role in the O_3 formation than the rest three sources,
328 with the O_3 contribution of 10 ~ 50 μg m^{-3} in the afternoon in Eastern China. In highly
329 industrialized areas, such as Hebei, Tianjin, Shandong, Zhejiang, et al., the O_3 contribution of
330 the industry source exceeds 30 μg m^{-3}. The residential source is not important in the O_3
331 formation, and contributes about 2 ~ 15 μg m^{-3} O_3 generally. The transportation source plays
332 a considerable role in the O_3 formation, accounting for about 5 ~ 30 μg m^{-3} O_3 in Eastern
333 China. The O_3 enhancement due to biogenic emissions is mainly concentrated in NCPs and
334 PRDs, particularly in PRDs, with the O_3 contribution of around 5 ~ 50 μg m^{-3}.
335 In order to further evaluate the contribution of various sources to the [O_3], the hourly
336 near-surface [O_3] in the control simulation are first subdivided into 16 bins with the interval
337 of 20 μg m^{-3}. [O_3] in the control and sensitivity simulations as the bin [O_3] are assembled
338 respectively, and an average of [O_3] in each bin are calculated. Figures 9 shows the
339 contributions of various emissions sources to [O_3] in the four sections of Eastern China

during the episode. The industry emission plays the most important role in the O_3 formation, and is the culprit of the high O_3 pollution. When the [O_3] in the control simulation are less than 100 μg m^{-3}, the industry source generally decreases [O_3]. However, when the simulated [O_3] are more than around 200 μg m^{-3}, the O_3 contribution from the industry emissions generally exceeds 50 μg m^{-3}, and when the simulated [O_3] are more than 300 μg m^{-3}, the industrial O_3 contribution can be up to 100 μg m^{-3}, constituting one third of the [O_3]. The O_3 contribution from the residential source is not significant, generally less than 20 μg m^{-3}. The transportation source plays the second most important role in the O_3 formation in NEC, NCPs, and YRDs, but its O_3 contribution is much less than that from the industry source when the simulated [O_3] are more than 150 μg m^{-3}. VOCs from the biogenic source generally enhance the O_3 formation, providing a background O_3 source. The biogenic source contributes about 10 ~ 50 μg m^{-3} O_3 when simulated [O_3] are more than 150 μg m^{-3} in NEC, NCPs, and YRDs. However, in PRDs, the biogenic emissions constitute the second most important O_3 source, with the O_3 contribution exceeding 50 μg m^{-3} when simulated [O_3] are more than 250 μg m^{-3}. Apparently, controlling the industry emissions can substantially mitigate the severer O_3 pollution in Eastern China. If the industry emissions are not considered in model simulations, on average, the [O_3] are generally not more than 200 μg m^{-3} in NEC, YRDs, and PRDs, but still can exceed 160 μg m^{-3}. In addition, excluding the industry source in NCPs does not mitigate [O_3] as remarkably as in the other regions, indicating that other emission sources also play an important role in the O_3 formation. Although the transportation emission is the second most important O_3 source in NEC, NCPs, and PRDs, its O_3 contribution is much less than that from the industry source. SI-Table 1 further presents the emission rates of major O_3 precursors from different emissions sources in the model domain during the study episode. The industrial source dominates the VOCs and NO_x emissions, playing a key role in the O_3

364 formation. The transportation source emits more NOx and active VOCs, such as olefins and
365 aromatics, than the residential source, contributing considerably to the O_3 formation.

366 Another three sensitivity studies are conducted to further explore the high O_3 formation
367 in Eastern China, in which only the industry, residential, and transportation source is
368 considered, respectively. It is worth to note that biogenic emissions are included in all the
369 three sensitivity simulations considering that the biogenic emissions provide natural O_3
370 precursors and cannot be anthropogenically controlled. Figure 10 presents the O_3
371 contributions from individual anthropogenic source averaged in the afternoon during the
372 whole episode in the four sections of Eastern China. If only the industry source is considered
373 or the residential and transportation sources are excluded in the simulation, Eastern China
374 still experiences high O_3 pollution. The O_3 contribution of the residential and transportation
375 sources are less than 60 μg m^{-3} on average, further showing the important role of the industry
376 source in the O_3 pollution. When the industry and residential sources are not considered in
377 the simulation, the transportation source still causes the simulated [O_3] to exceed 160 μg m^{-3},
378 particularly in NCPs. Taking into consideration the very fast increase of vehicles in China
379 recently (X. Wu et al., 2016), the transportation source increasingly constitutes a more
380 important O_3 source, particularly when the industry source is under control. Apparently,
381 when the industry and transportation sources are excluded or only residential source is
382 included, the high O_3 pollution is significantly mitigated and the simulated [O_3] are less than
383 160 μg m^{-3} on average. Figure 11 provides the distribution of the [O_3] averaged during the
384 peak time on May 25 when the most serous O_3 pollution occurs during the simulated episode.
385 When only the industry emissions are considered, the O_3 pollution is mitigated considerably
386 in Eastern China, but still widespread in NCPs and PRDs. If only considering the
387 transportation source, the O_3 pollution still occurs in NCPs, with the [O_3] exceeding 160 μg
388 m^{-3}. When the industry and transportation sources are excluded, the O_3 pollution is generally

under control. Hence, reducing the emissions from industry and transportation is a key to mitigate O_3 pollution in Eastern China.

4 Summary and Conclusions

In the present study, air pollutants observations, released by China MEP, have been analyzed to explore the O_3 pollution situation in Eastern China. Analyses of air pollutants observations in 66 cities from 2013 to 2015 have shown that, although implementation of the APPCAP has considerably decreased the CO, SO_2, NO_2, and $PM_{2.5}$ mass concentrations from April to September in Eastern China, the [O_3] have increased by 9.2% and the frequency of O_3 exceedance with hourly [O_3] exceeding 200 μg m^{-3} has increased by about 25% in the afternoon. Mitigation of NO_x and $PM_{2.5}$ due to implementation of the APPCAP, increasing transportation activities, or variability of meteorological situations perhaps contributes to the deterioration of the O_3 pollution in Eastern China.

O_3 observations from April to September in 2015 have shown that Eastern China has experienced widespread and persistent O_3 pollution. Only two cities in Eastern China have observed the maximum 1-h [O_3] less than 200 μg m^{-3}. Over 25% of cities have observed the maximum 1-h [O_3] exceeding 400 μg m^{-3}, particularly more than 800 μg m^{-3} [O_3] have been observed in six cities in Eastern China. The average daily maximum 1-h [O_3] from April to September exceed 160 μg m^{-3} in 45% of cities in Eastern China, and the 1-h [O_3] of 200 μg m^{-3} have been exceeded on over 10% of days from April to September in 129 cities, and on 40% of days in 10 cities.

A widespread and severe O_3 pollution episode from 22 to 28 May 2015 in Eastern China has been simulated using the WRF-CHEM model. The model generally simulates reasonably well the temporal variations and spatial distributions of near-surface [O_3], but the uncertainties of meteorological fields or emission inventories still cause model

414 overestimation or underestimation. The model performs reasonably in simulating NO_2, but
415 the model biases are rather large during nighttime.

416 FSA is utilized to assess the O_3 contribution of biogenic and various anthropogenic
417 sources. Sensitivity studies have shown that the industry source plays the most important role
418 in the O_3 pollution formation. When the simulated [O_3] are more than around 200 μg m^{-3}, the
419 O_3 contribution from the industry emissions generally exceeds 50 μg m^{-3} in Eastern China,
420 particularly when the simulated [O_3] exceed 300 μg m^{-3}, the industrial O_3 contribution
421 constitutes one third of the [O_3]. The transportation emission is the second most important O_3
422 source in NEC, YRDs, and PRDs, but its O_3 contribution is much less than that from the
423 industry source when the simulated [O_3] exceed 150 μg m^{-3}. The biogenic source plays a
424 more important role in O_3 formation than the transportation source in PRDs, with the O_3
425 contribution exceeding 50 μg m^{-3} when simulated [O_3] are more than 250 μg m^{-3}. In general,
426 the O_3 contribution from residential source is not significant. Further sensitivity studies have
427 also indicated that if only considering the residential source or excluding the industry and
428 transportation sources in simulations, the O_3 pollution in Eastern China could be significantly
429 improved. Only the industry or transportation source still causes O_3 pollution, particularly
430 with regard to the industry source.

431 Widespread and persistent O_3 pollution poses adverse impacts on ecosystems and
432 human health. Considering the key role of the industry source in the high O_3 formation,
433 mitigation of the industry source becomes the top choice to improve the O_3 pollution in
434 Eastern China, particularly with regard to the VOCs emissions that are still not fully
435 considered in the current air pollutant control strategy. Rapid increase of vehicles also
436 enhances the VOCs and NO_x emissions and the transportation source plays an increasingly
437 important role in the O_3 pollution. In addition, the rapid decrease of $PM_{2.5}$ due to
438 implementation of the APPCAP reduces the aerosol and cloud optical depth, which is subject

to enhance the O_3 formation by increasing the photolysis. Hence, stringent control strategies of VOCs and NO_x need to be designed comprehensively and implemented to avoid the looming severe O_3 pollution in Eastern China.

Although the model performs generally well in simulating O_3 and NO_2 during a seven-day O_3 pollution episode in Eastern China, uncertainties from meteorological fields simulations and emissions inventory still cause model biases. Meteorological conditions play a key role in the formation of air pollution, determining the formation, transformation, diffusion, transport, and removal of the air pollutants in the atmosphere (Bei et al., 2010, 2012). A nudging of wind and temperature fields using observations generally improves the simulation of meteorological fields, reducing the model biases in reproducing the O_3 temporal variation and spatial distribution. So future studies are needed to improve the meteorological fields using the data assimilation, such as the four-dimension data assimilation (FDDA). Taking into consideration the complexity of the O_3 formation and rapid changes of emissions inventories, further model studies need to be performed to investigate the O_3 formation for supporting the design and implementation of emission control strategies, based on the improved meteorological fields simulations.

Acknowledgements. This work was supported by the National Natural Science Foundation of China (No. 41275153) and by the "Strategic Priority Research Program" of the Chinese Academy of Sciences，Grant No. XDB05060500. Guohui Li is also supported by the “Hundred Talents Program” of the Chinese Academy of Sciences. Naifang Bei is supported by the National Natural Science Foundation of China (No. 41275101). Wenting Dai is supported by the National Natural Science Foundation of China (No. 41503117).

463 **Reference**

464 Banta, R. M., Senff, C. J., Nielsen-Gammon, J., Darby, L. S., Ryerson, T. B., Alvarez, R. J.,
465 Sandberg, S. R., Williams, E. J., and Trainer, M.: A bad air day in Houston, Bull. Amer.
466 Meteorol. Soc., 86, 657-669, 10.1175/bams-86-5-657, 2005.

467 Bei, N., Lei, W., Zavala, M., and Molina, L. T.: Ozone predictabilities due to meteorological
468 uncertainties in the Mexico City basin using ensemble forecasts, Atmos. Chem. Phys., 10,
469 6295-6309, 10.5194/acp-10-6295-2010, 2010.

470 Bei, N., Li, G., and Molina, L. T.: Uncertainties in SOA simulations due to meteorological
471 uncertainties in Mexico City during MILAGRO-2006 field campaign, Atmos. Chem.
472 Phys., 12, 11295-11308, 10.5194/acp-12-11295-2012, 2012.

473 Bell, M. L., Peng, R. D., and Dominici, F.: The exposure-response curve for ozone and risk
474 of mortality and the adequacy of current ozone regulations, Environ. Health Persp., 114,
475 532-536, 10.1289/ehp.8816, 2006.

476 Binkowski, F. S., and Roselle, S. J.: Models-3 community multiscale air quality (CMAQ)
477 model aerosol component - 1. Model description, J. Geophys. Res., 108, 18,
478 10.1029/2001jd001409, 2003.

479 Brasseur, G. P., Orlando, J. J., and Tyndall, G. S.: Atmospheric chemistry and global change,
480 Oxford University Press, Cambridge, USA, 654 pp., 1999.

481 Cao, J. J., Xu, H. M., Xu, Q., Chen, B. H., and Kan, H. D.: Fine Particulate Matter
482 Constituents and Cardiopulmonary Mortality in a Heavily Polluted Chinese City, Environ.
483 Health Persp., 120, 373-378, 10.1289/ehp.1103671, 2012.

484 Calkins, C., Ge, C., Wang, J., Anderson, M., and Yang, K.: Effects of meteorological
485 conditions on sulfur dioxide air pollution in the North China Plain during winters of
486 2006-2015, Atmospheric Environment, 296-309, 2016.

487 Chameides, W. L., Lindsay, R. W., Richardson, J., and Kiang, C. S.: The role of biogenic
488 hydrocarbons in urban photochemical smog - Atlanta as a case-study, Science, 241, 1473-
489 1475, 10.1126/science.3420404, 1988.

490 Chen, F., and Dudhia, J.: Coupling an advanced land surface-hydrology model with the Penn
491 State-NCAR MM5 modeling system. Part I: Model implementation and sensitivity, Mon.
492 Weather Rev., 129, 569-585, 10.1175/1520-0493(2001)129<0569:caalsh>2.0.co;2, 2001.

493 Chen, W., Yan, L., and Zhao, H. M.: Seasonal Variations of Atmospheric Pollution and Air
494 Quality in Beijing, Atmosphere, 6, 1753-1770, 10.3390/atmos6111753, 2015.

495 Cheng, N., Li, Y., Zhang, D., Chen, T., Sun, F., Chen, C., and Meng, F.: Characteristics of
496 Ground Ozone Concentration over Beijing from 2004 to 2015: Trends, Transport, and
497 Effects of Reductions, Atmos. Chem. Phys. Discuss., 2016, 1-21, 10.5194/acp-2016-508,
498 2016.

499 Chou, M.-D. and M. J. Suarez: A solar radiation parameterization for atmospheric studies,
500 NASA Tech. Rep. NASA/TM-1999-10460, 15, 38 pp, 1999.

501 Chou, M.-D. and M. J. Suarez: A thermal infrared radiation parameterization for atmospheric
502 studies, NASA/TM-2001-104606, 19, 55 pp, 2001.

503 Feng, T., Bei, N., Huang, R. J., Cao, J., Zhang, Q., Zhou, W., Tie, X., Liu, S., Zhang, T., Su,
504 X., Lei, W., Molina, L. T., and Li, G.: Summertime ozone formation in Xi'an and

surrounding areas, China, Atmos. Chem. Phys., 16, 4323-4342, 10.5194/acp-16-4323-2016, 2016.

Grell, G. A., Peckham, S. E., Schmitz, R., McKeen, S. A., Frost, G., Skamarock, W. C., and Eder, B.: Fully coupled "online" chemistry within the WRF model, Atmos. Environ., 39, 6957-6975, 10.1016/j.atmosenv.2005.04.027, 2005.

Guenther, A., Karl, T., Harley, P., Wiedinmyer, C., Palmer, P. I., and Geron, C.: Estimates of global terrestrial isoprene emissions using MEGAN (Model of Emissions of Gases and Aerosols from Nature), Atmos. Chem. Phys., 6, 3181-3210, 2006.

Huang, M., Carmichael, G. R., Spak, S. N., Adhikary, B., Kulkarni, S., Cheng, Y., Wei, C., Tang, Y., D'Allura, A., Wennberg, P. O., Huey, G. L., Dibb, J. E., Jimenez, J. L., Cubison, M. J., Weinheimer, A. J., Kaduwela, A., Cai, C., Wong, M., Pierce, R. B., Al-Saadi, J. A., Streets, D. G., and Zhang, Q.: Multi-scale modeling study of the source contributions to near-surface ozone and sulfur oxides levels over California during the ARCTAS-CARB period, Atmos. Chem. Phys., 11, 3173-3194, 10.5194/acp-11-3173-2011, 2011.

Huang, J., Liu, H., Crawford, J. H., Chan, C., Considine, D. B., Zhang, Y., Zheng, X., Zhao, C., Thouret, V., Oltmans, S. J., Liu, S. C., Jones, D. B. A., Steenrod, S. D., and Damon, M. R.: Origin of springtime ozone enhancements in the lower troposphere over Beijing: in situ measurements and model analysis, Atmos. Chem. Phys., 15, 5161-5179, 10.5194/acp-15-5161-2015, 2015.

Hong, S.-Y., and Lim, J.-O. J.: The WRF Single-Moment 6-Class Microphysics Scheme (WSM6), Asia-Pacific Journal of Atmospheric Sciences, 42, 129-151, 2006.

Horowitz, L. W., Walters, S., Mauzerall, D. L., Emmons, L. K., Rasch, P. J., Granier, C., Tie, X. X., Lamarque, J. F., Schultz, M. G., Tyndall, G. S., Orlando, J. J., and Brasseur, G. P.: A global simulation of tropospheric ozone and related tracers: Description and evaluation of MOZART, version 2, J. Geophys. Res., 108, 29, 10.1029/2002jd002853, 2003.

Janjić, Z. I.: Nonsingular Implementation of the Mellor–Yamada Level 2.5 Scheme in the NCEP Meso Model, Ncep Office Note, 436, 2002.

Kurokawa, J., Ohara, T., Morikawa, T., Hanayama, S., Janssens-Maenhout, G., Fukui, T., Kawashima, K., and Akimoto, H.: Emissions of air pollutants and greenhouse gases over Asian regions during 2000-2008: Regional Emission inventory in ASia (REAS) version 2, Atmos. Chem. Phys., 13, 11019-11058, 10.5194/acp-13-11019-2013, 2013.

Li, G., Zhang, R., Fan, J., and Tie, X.: Impacts of black carbon aerosol on photolysis and ozone, J. Geophys. Res., 110, 10.1029/2005jd005898, 2005.

Li, G., Zhang, R., Fan, J., and Tie, X.: Impacts of biogenic emissions on photochemical ozone production in Houston, Texas, J. Geophys. Res., 112, 10.1029/2006jd007924, 2007.

Li, G., Lei, W., Zavala, M., Volkamer, R., Dusanter, S., Stevens, P., and Molina, L. T.: Impacts of HONO sources on the photochemistry in Mexico City during the MCMA-2006/MILAGO Campaign, Atmos. Chem. Phys., 10, 6551-6567, 10.5194/acp-10-6551-2010, 2010.

Li, G., Bei, N., Tie, X., and Molina, L. T.: Aerosol effects on the photochemistry in Mexico City during MCMA-2006/MILAGRO campaign, Atmos. Chem. Phys., 11, 5169-5182, 10.5194/acp-11-5169-2011, 2011a.

Li, G., Zavala, M., Lei, W., Tsimpidi, A. P., Karydis, V. A., Pandis, S. N., Canagaratna, M. R., and Molina, L. T.: Simulations of organic aerosol concentrations in Mexico City using

549 the WRF-CHEM model during the MCMA-2006/MILAGRO campaign, Atmos. Chem.
550 Phys., 11, 3789-3809, 10.5194/acp-11-3789-2011, 2011b.

551 Li, G., Lei, W., Bei, N., and Molina, L. T.: Contribution of garbage burning to chloride and
552 PM2.5 in Mexico City, Atmos. Chem. Phys., 12, 8751-8761, 10.5194/acp-12-8751-2012,
553 2012.

554 Li, G., Bei, N. F., Zavala, M., and Molina, L. T.: Ozone formation along the California
555 Mexican border region during Cal-Mex 2010 field campaign, Atmos. Environ., 88, 370-
556 389, 10.1016/j.atmosenv.2013.11.067, 2014.

557 Liu, Z., Wang, Y., Gu, D., Zhao, C., Huey, L. G., Stickel, R., Liao, J., Shao, M., Zhu, T.,
558 Zeng, L., Amoroso, A., Costabile, F., Chang, C. C., and Liu, S. C.: Summertime
559 photochemistry during CAREBeijing-2007: RO_x budgets and O_3 formation, Atmos.
560 Chem. Phys., 12, 7737-7752, 10.5194/acp-12-7737-2012, 2012.

561 Lippmann, M.: Health-effects of tropospheric ozone - review of recent research findings and
562 their implications to ambient air-quality standards, J. Expo. Anal. Environ. Epidemiol., 3,
563 103-129, 1993.

564 Ma, Z. Q., Xu, J., Quan, W. J., Zhang, Z. Y., Lin, W. L., and Xu, X. B.: Significant increase
565 of surface ozone at a rural site, north of eastern China, Atmos. Chem. Phys., 16, 3969-
566 3977, 2016.

567 National Research Council (1991), Rethinking the Ozone Problem in Urban and Regional Air
568 Pollution, National Academy Press, Washington, D.C.

569 Nenes, A., Pandis, S. N., and Pilinis, C.: ISORROPIA: A new thermodynamic equilibrium
570 model for multiphase multicomponent inorganic aerosols, Aquat. Geochem., 4, 123-152,
571 10.1023/a:1009604003981, 1998.

572 Oikawa, P.Y. , Ge, C., Wang, J., Eberwein, J. R., Liang, L. L., Allsman, L. A., Grantz, D. A.,
573 and Jenerette, G. D.: 2015. Unusually high soil nitrogen oxide emissions influence air
574 quality in a high-temperature agricultural region, Nat. Commun., 6, 8753-8757, 2015.

575 Ou, J. M., Yuan, Z. B., Zheng, J. Y., Huang, Z. J., Shao, M., Li, Z. K., Huang, X. B., Guo, H.,
576 and Louie, P. K. K.: Ambient Ozone Control in a Photochemically Active Region: Short
577 Term Despiking or Long-Term Attainment?, Environ. Sci. Technol., 50, 5720-5728,
578 10.1021/acs.est.6b00345, 2016.

579 Richter, A., Burrows, J. P., Nuss, H., Granier, C., and Niemeier, U.: Increase in tropospheric
580 nitrogen dioxide over China observed from space, Nature, 437, 129-132,
581 10.1038/nature04092, 2005.

582 Shan, Y., Li, L., Liu, Q., Chen, Y., Shi, Y., Liu, X., and Qiao, L.: Spatial-Temporal
583 Distribution of ozone and its precursors over central and eastern China based on OMI
584 Data, Res. Environ. Sci., 29, 1128-1136, 2016.

585 Situ, S., Guenther, A., Wang, X., Jiang, X., Turnipseed, A., Wu, Z., Bai, J., and Wang, X.:
586 Impacts of seasonal and regional variability in biogenic VOC emissions on surface ozone
587 in the Pearl River delta region, China, Atmos. Chem. Phys., 13, 11803-11817,
588 10.5194/acp-13-11803-2013, 2013.

589 Tao, Z. N., Larson, S. M., Wuebbles, D. J., Williams, A., and Caughey, M.: A summer
590 simulation of biogenic contributions to ground-level ozone over the continental United
591 States, J. Geophys. Res., 108, 24, 10.1029/2002jd002945, 2003.

592 Tie, X., Geng, F., Guenther, A., Cao, J., Greenberg, J., Zhang, R., Apel, E., Li, G.,
593 Weinheimer, A., Chen, J., and Cai, C.: Megacity impacts on regional ozone formation:
594 observations and WRF-Chem modeling for the MIRAGE-Shanghai field campaign,
595 Atmos. Chem. Phys., 13, 5655-5669, 10.5194/acp-13-5655-2013, 2013.

596 Tie, X. X., Madronich, S., Walters, S., Zhang, R. Y., Rasch, P., and Collins, W.: Effect of
597 clouds on photolysis and oxidants in the troposphere, J. Geophys. Res., 108, 25,
598 10.1029/2003jd003659, 2003.

599 Tie, X., Geng, F., Guenther, A., Cao, J., Greenberg, J., Zhang, R., Apel, E., Li, G.,
600 Weinheimer, A., Chen, J., and Cai, C.: Megacity impacts on regional ozone formation:
601 observations and WRF-Chem modeling for the MIRAGE-Shanghai field campaign,
602 Atmos. Chem. Phys., 13, 5655-5669, 10.5194/acp-13-5655-2013, 2013.

603 Wang, J., Ge, C., Yang, Z., Hyer, E. J., Reid, J. S., Chew, B.-N., Mahmud, M., Zhang, Y.,
604 and Zhang, M.: Mesoscale modeling of smoke transport over the Southeast Asian
605 Maritime Continent: interplay of sea breeze, trade wind, typhoon, and topography, Atmos.
606 Res., 122, 486-503, 2013.

607 Wang, S. W., Zhang, Q., Streets, D. G., He, K. B., Martin, R. V., Lamsal, L. N., Chen, D.,
608 Lei, Y., and Lu, Z.: Growth in NOx emissions from power plants in China: bottom-up
609 estimates and satellite observations, Atmos. Chem. Phys., 12, 4429-4447, 10.5194/acp-
610 12-4429-2012, 2012.

611 Wang, T., Ding, A. J., Gao, J., and Wu, W. S.: Strong ozone production in urban plumes
612 from Beijing, China, Geophys. Res. Lett., 33, 5, 10.1029/2006gl027689, 2006.

613 Wang, X., Zhang, Y., Hu, Y., Zhou, W., Lu, K., Zhong, L., Zeng, L., Shao, M., Hu, M., and
614 Russell, A. G.: Process analysis and sensitivity study of regional ozone formation over
615 the Pearl River Delta, China, during the PRIDE-PRD2004 campaign using the
616 Community Multiscale Air Quality modeling system, Atmos. Chem. Phys., 10, 4423-
617 4437, 10.5194/acp-10-4423-2010, 2010.

618 Wang, Y., Zhang, Q. Q., He, K., Zhang, Q., and Chai, L.: Sulfate-nitrate-ammonium aerosols
619 over China: response to 2000-2015 emission changes of sulfur dioxide, nitrogen oxides,
620 and ammonia, Atmos. Chem. Phys., 13, 2635-2652, 10.5194/acp-13-2635-2013, 2013.

621 Wang, Z., Zeng, H., Wei, Y., and Zhang, Y.: Regional total factor energy efficiency: An
622 empirialcal analysis of inudstrial sectior in China, Appl. Energ., 2012, 97, 115-123, 2012.

623 Weinhold, B.: Ozone nation - EPA standard panned by the people, Environ. Health Persp.,
624 116, A302-A305, 2008.

625 Wesely, M. L.: Parameterization of surface resistances to gaseous dry deposition in regional-
626 scale numerical models, Atmos. Environ., 23, 1293-1304, http://dx.doi.org/10.1016/0004-
627 6981(89)90153-4, 1989.

628 Wu, J., Li, G., Cao, J., Bei, N., Wang, Y., Feng, T., Huang, R., Liu, S., Zhang, Q., and Tie, X.:
629 Contributions of Trans-boundary Transport to the Summertime Air Quality in Beijing,
630 China, Atmos. Chem. Phys. Discuss., 2016, 1-46, 10.5194/acp-2016-705, 2016.

631 Wu, X., Wu, Y., Zhang, S., Liu, H., Fu, L., and Hao, J.: Assessment of vehicle emission
632 programs in China during 1998-2013: Achievement, challlenges and implications,
633 Environ. Pollut., 2016, 214, 556-567, 2016.

634 Xing, J., Wang, S. X., Chatani, S., Zhang, C. Y., Wei, W., Hao, J. M., Klimont, Z., Cofala, J.,
635 and Amann, M.: Projections of air pollutant emissions and its impacts on regional air

quality in China in 2020, Atmos. Chem. Phys., 11, 3119-3136, 10.5194/acp-11-3119-2011, 2011.

Xu J, Ma J Z, Zhang X L, et al. Measurements of ozone and its precursors in Beijing during summertime: impact of urban plumes on ozone pollution in downwind rural areas, Atmos. Chem. Phys., 2011, 11, 12241-12252.

Yang, X. F., Liu, H., Man, H. Y., and He, K. B.: Characterization of road freight transportation and its impact on the national emission inventory in China, Atmos. Chem. Phys., 15, 2105-2118, doi:10.5194/acp-15-2105-2015, 2015.

Xue, L. K., Wang, T., Gao, J., Ding, A. J., Zhou, X. H., Blake, D. R., Wang, X. F., Saunders, S. M., Fan, S. J., Zuo, H. C., Zhang, Q. Z., and Wang, W. X.: Ground-level ozone in four Chinese cities: precursors, regional transport and heterogeneous processes, Atmos. Chem. Phys., 14, 13175-13188, 10.5194/acp-14-13175-2014, 2014.

Zhang, Q., Streets, D. G., Carmichael, G. R., He, K. B., Huo, H., Kannari, A., Klimont, Z., Park, I. S., Reddy, S., Fu, J. S., Chen, D., Duan, L., Lei, Y., Wang, L. T., and Yao, Z. L.: Asian emissions in 2006 for the NASA INTEX-B mission, Atmos. Chem. Phys., 9, 5131–5153, doi:10.5194/acp-9-5131-2009, 2009.

Zhou, J. A., Ito, K., Lall, R., Lippmann, M., and Thurston, G.: Time-Series Analysis of Mortality Effects of Fine Particulate Matter Components in Detroit and Seattle, Environ. Health Persp., 119, 461-466, 10.1289/ehp.1002613, 2011.

657 Table 1 WRF-CHEM model configurations
658

Regions	**Eastern China**
Simulation period	May 22 to 28, 2015
Domain size	350 × 350
Domain center	35°N, 114°E
Horizontal resolution	10km × 10km
Vertical resolution	35 vertical levels with a stretched vertical grid with spacing ranging from 30 m near the surface, to 500 m at 2.5 km and 1 km above 14 km
Microphysics scheme	WSM 6-class graupel scheme (Hong and Lim, 2006)
Boundary layer scheme	MYJ TKE scheme (Janjić, 2002)
Surface layer scheme	MYJ surface scheme (Janjić, 2002)
Land-surface scheme	Unified Noah land-surface model (Chen and Dudhia, 2001)
Longwave radiation scheme	Goddard longwave scheme (Chou and Suarez, 2001)
Shortwave radiation scheme	Goddard shortwave scheme (Chou and Suarez, 1999)
Meteorological boundary and initial conditions	NCEP 1°×1° reanalysis data
Chemical initial and boundary conditions	MOZART 6-hour output (Horowitz et al., 2003)
Anthropogenic emission inventory	SAPRC-99 chemical mechanism emissions (Zhang et al., 2009)
Biogenic emission inventory	MEGAN model developed by Guenther et al. (2006)
Model spin-up time	28 hours

659
660

661 Table 2 Observed hourly mass concentrations of pollutants averaged in the afternoon from
662 April to September 2013 and 2015 in 65 cities of Eastern China.
663

Pollutants	CO (mg m^{-3})	SO_2 (μg m^{-3})	NO_2 (μg m^{-3})	O_3 (μg m^{-3})	$PM_{2.5}$ (μg m^{-3})
2013	1.05	24.8	27.7	100.5	46.9
2015	0.77	15.4	23.9	110.5	38.2
Change (%)	-26.7	-37.8	-13.5	+9.9	-18.5

664
665

Figure Captions

Figure 1 WRF-CHEM simulation domain with topography. The filled circles represent centers of cities with ambient monitoring sites and the size of circles denotes the number of ambient monitoring sites of cities. The red and blue filled circles show the cities with air pollutants observations since 2013 and 2015, respectively.

Figure 2 Distribution of observed maximum 1-h [O_3] in Mainland China from April to September 2015.

Figure 3 Distribution of average daily maximum 1-h [O_3] in Mainland China from April to September 2015.

Figure 4 Distribution of days with the maximum 1-h [O_3] exceeding 160 μg m^{-3} in Mainland China from April to September 2015.

Figure 5 Distribution of days with the maximum 1-h [O_3] exceeding 200 μg m^{-3} in Mainland China from April to September 2015.

Figure 6 Pattern comparison of simulated vs. observed near-surface O_3 at 15:00 BJT from 22 to 27 May 2015. Colored circles: O_3 observations; color contour: O_3 simulations; black arrows: simulated surface winds.

Figure 7 Comparison of measured (black dots) and predicted (blue line) diurnal profiles of near-surface O_3 averaged over all ambient monitoring stations in provinces of Eastern China from 22 to 28 May 2015.

Figure 8 Distributions of the contribution to near-surface [O_3] averaged in the afternoon during the whole episode from (a) industry, (b) residential, (c) transportation, and (d) biogenic emissions.

Figure 9 O_3 contributions of industry (red line), residential (brown line), transportation (blue line), and biogenic emissions (green line) in NEC, NCPs, YRDs, and PRDs, as a function of simulated [O_3] in the control case.

Figure 10 O_3 contributions when only the industry (red line), residential (brown line), and transportation emissions (blue line) are considered in NEC, NCPs, YRDs, and PRDs, as a function of simulated [O_3] in the control case.

Figure 11 Distributions of the average O_3 concentration during peak time with (a) all anthropogenic emissions, (b) industry emissions alone, (c) residential emissions alone, and (d) transportation emissions alone on May 2015.

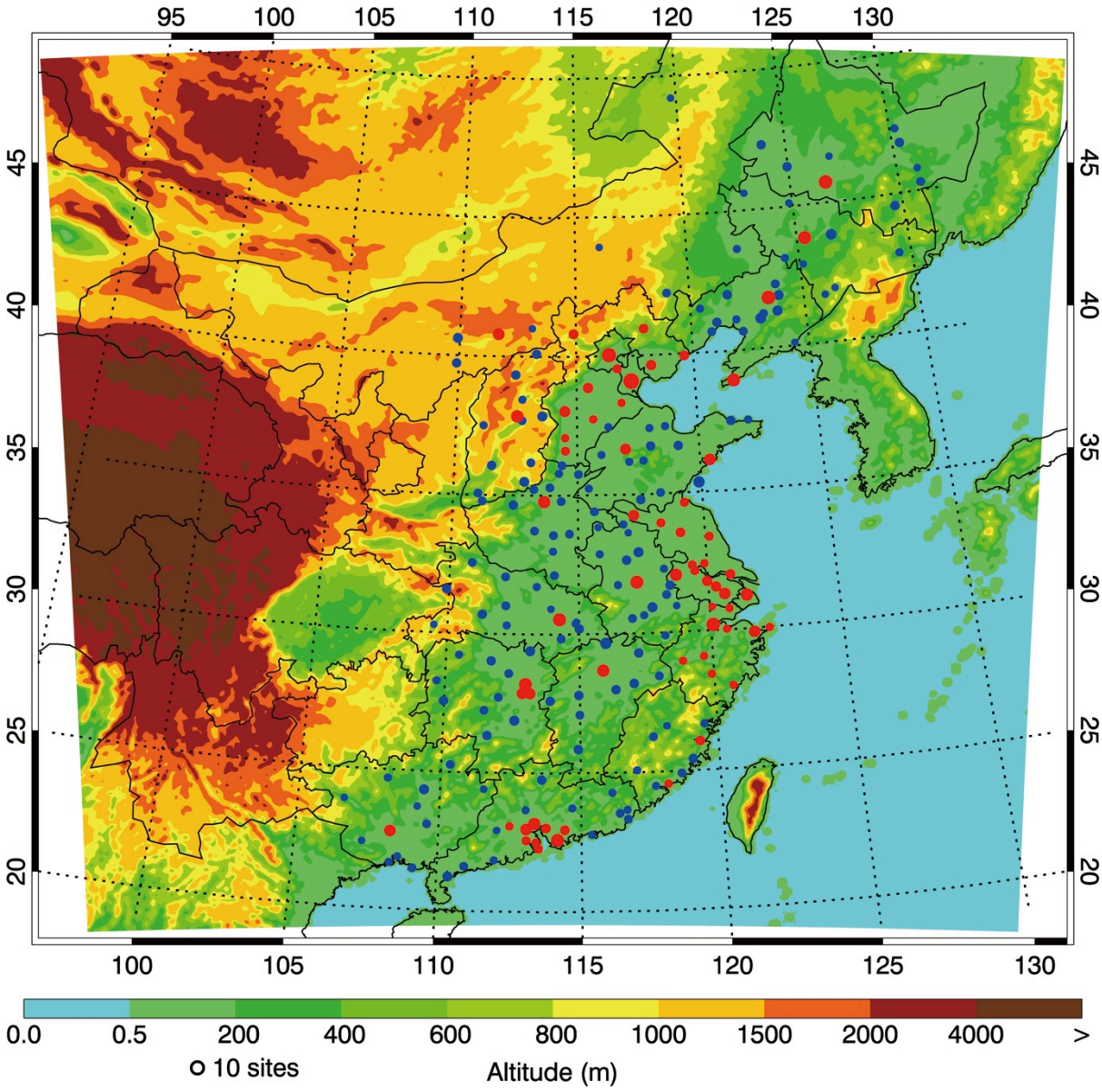

Figure 1 WRF-CHEM simulation domain with topography. The filled circles represent centers of cities with ambient monitoring sites and the size of circles denotes the number of ambient monitoring sites of cities. The red and blue filled circles show the cities with air pollutants observations since 2013 and 2015, respectively.

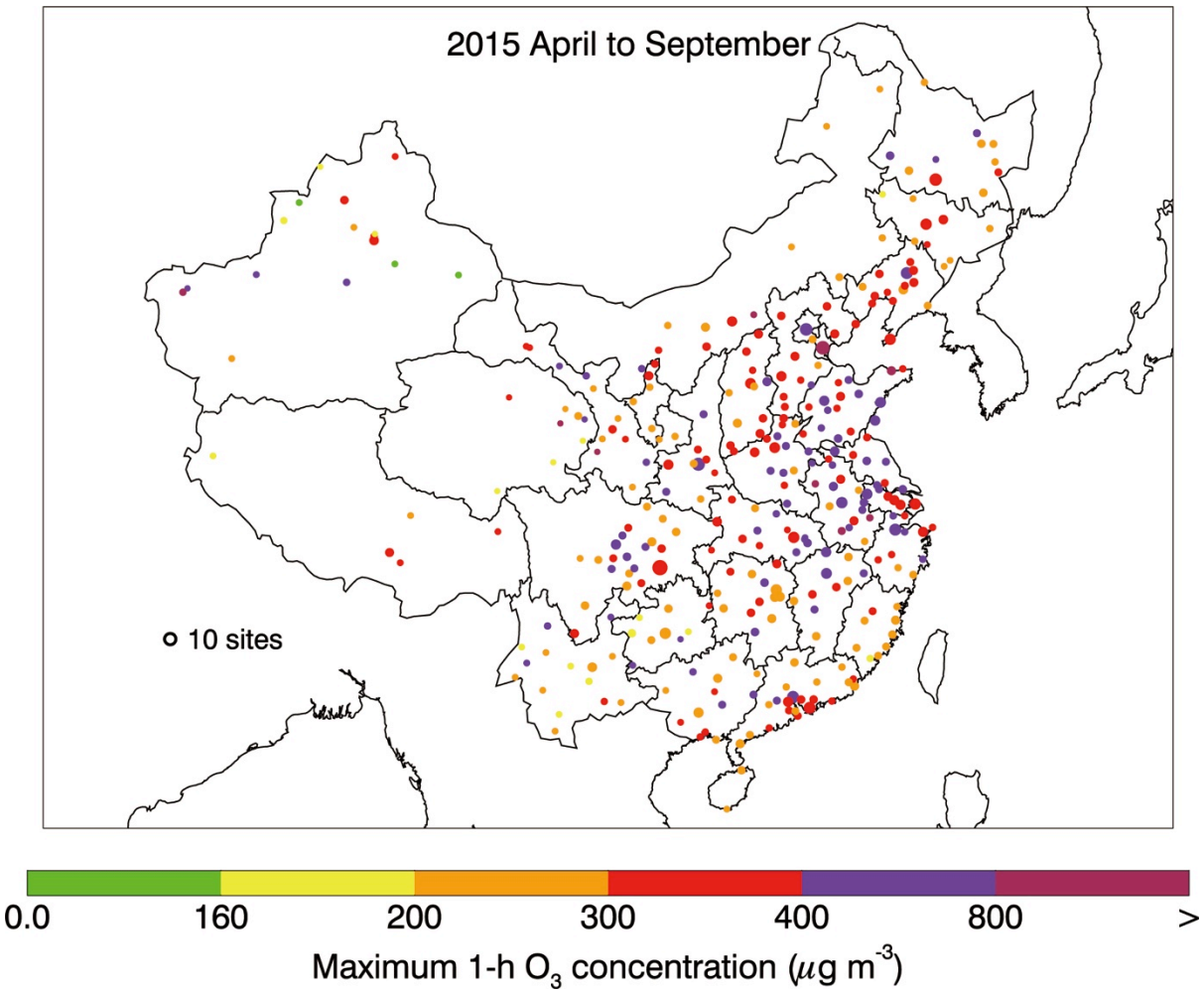

Figure 2 Distribution of observed maximum 1-h [O_3] in Mainland China from April to September 2015.

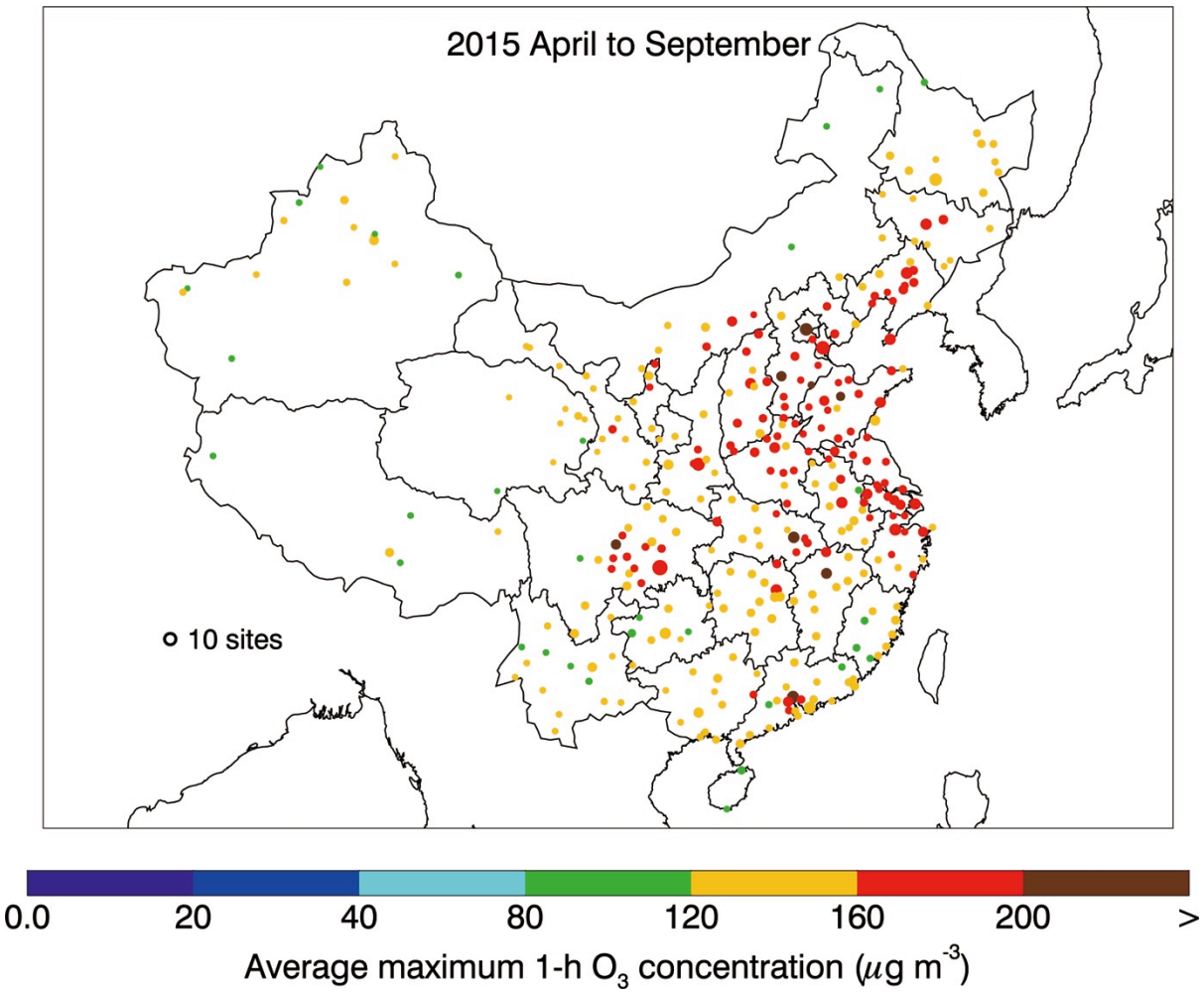

Figure 3 Distribution of average daily maximum 1-h [O_3] in Mainland China from April to September 2015.

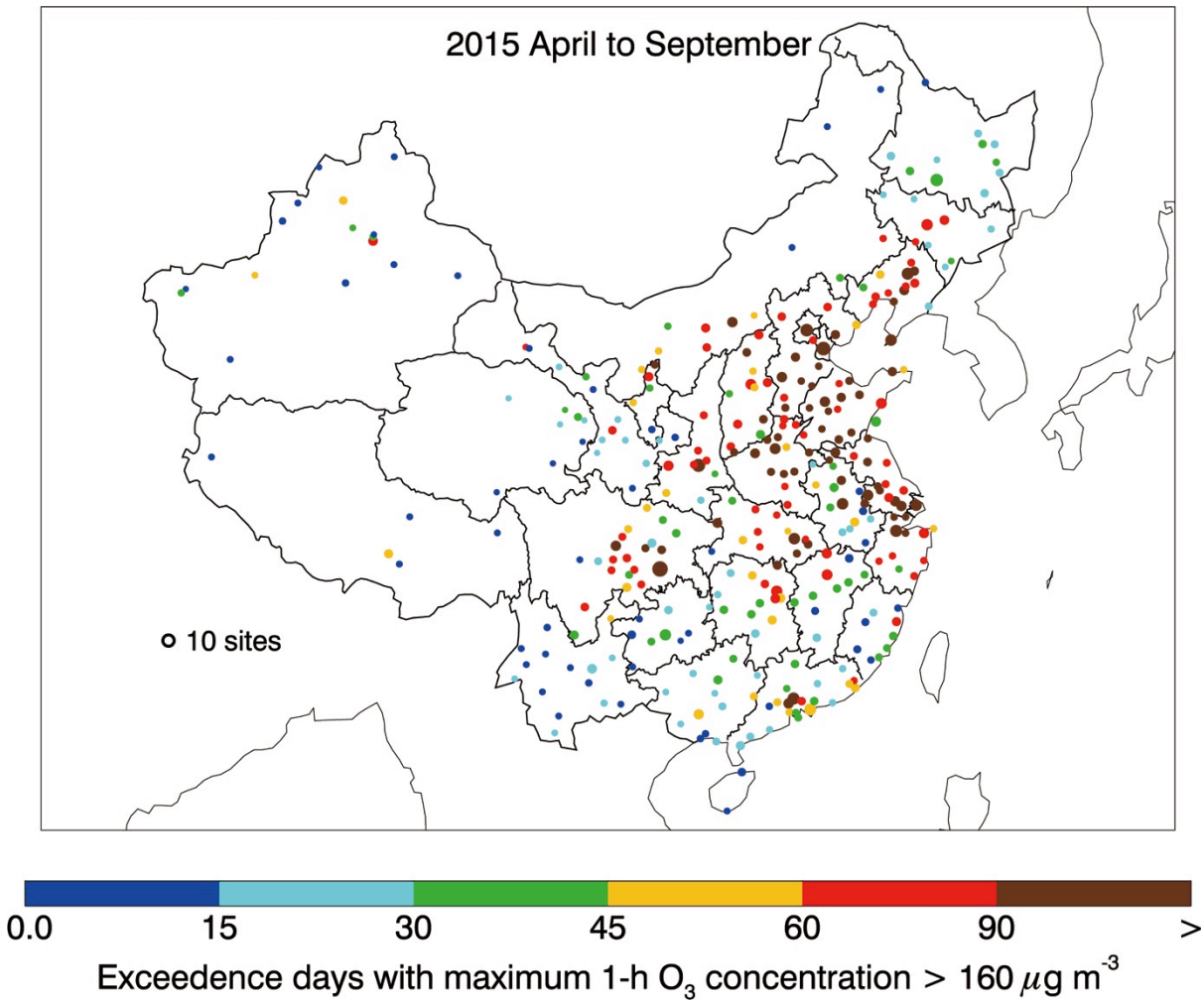

Figure 4 Distribution of days with the maximum 1-h [O_3] exceeding 160 μg m^{-3} in Mainland China from April to September 2015.

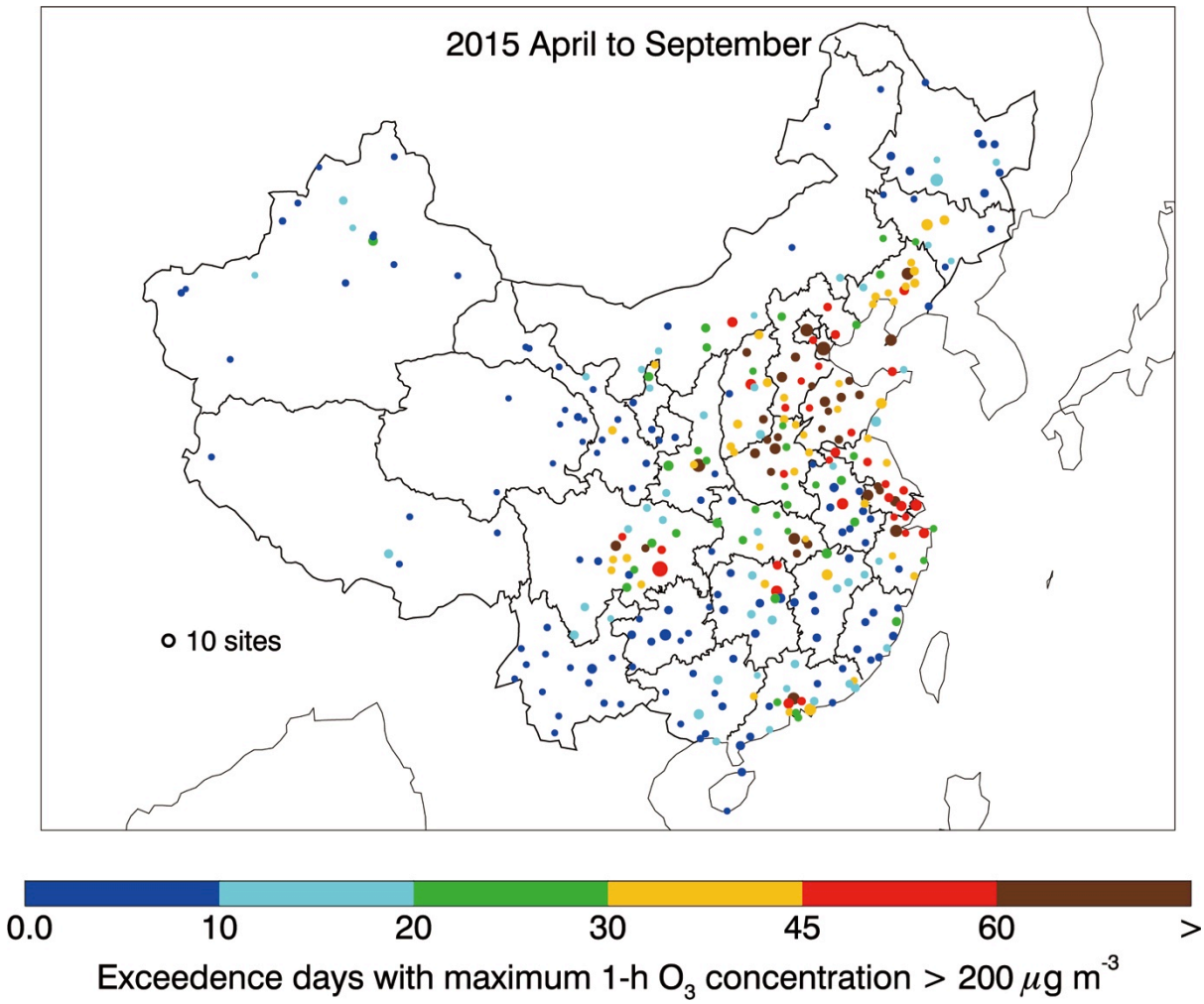

Figure 5 Distribution of days with the maximum 1-h [O_3] exceeding 200 μg m^{-3} in Mainland China from April to September 2015.

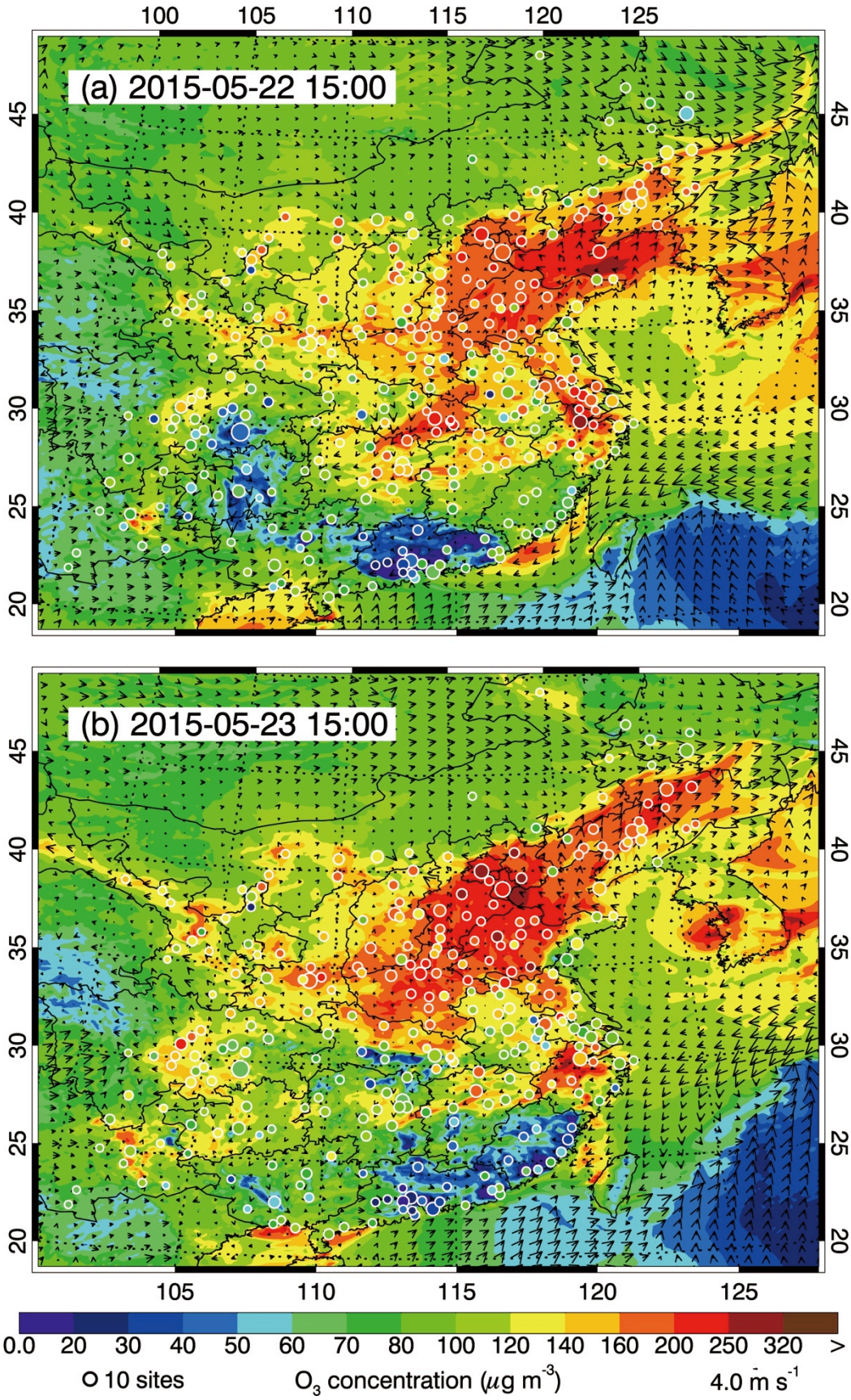

Figure 6 Pattern comparison of simulated vs. observed near-surface O_3 at 15:00 BJT from 22 to 27 May 2015. Colored circles: O_3 observations; color contour: O_3 simulations; black arrows: simulated surface winds.

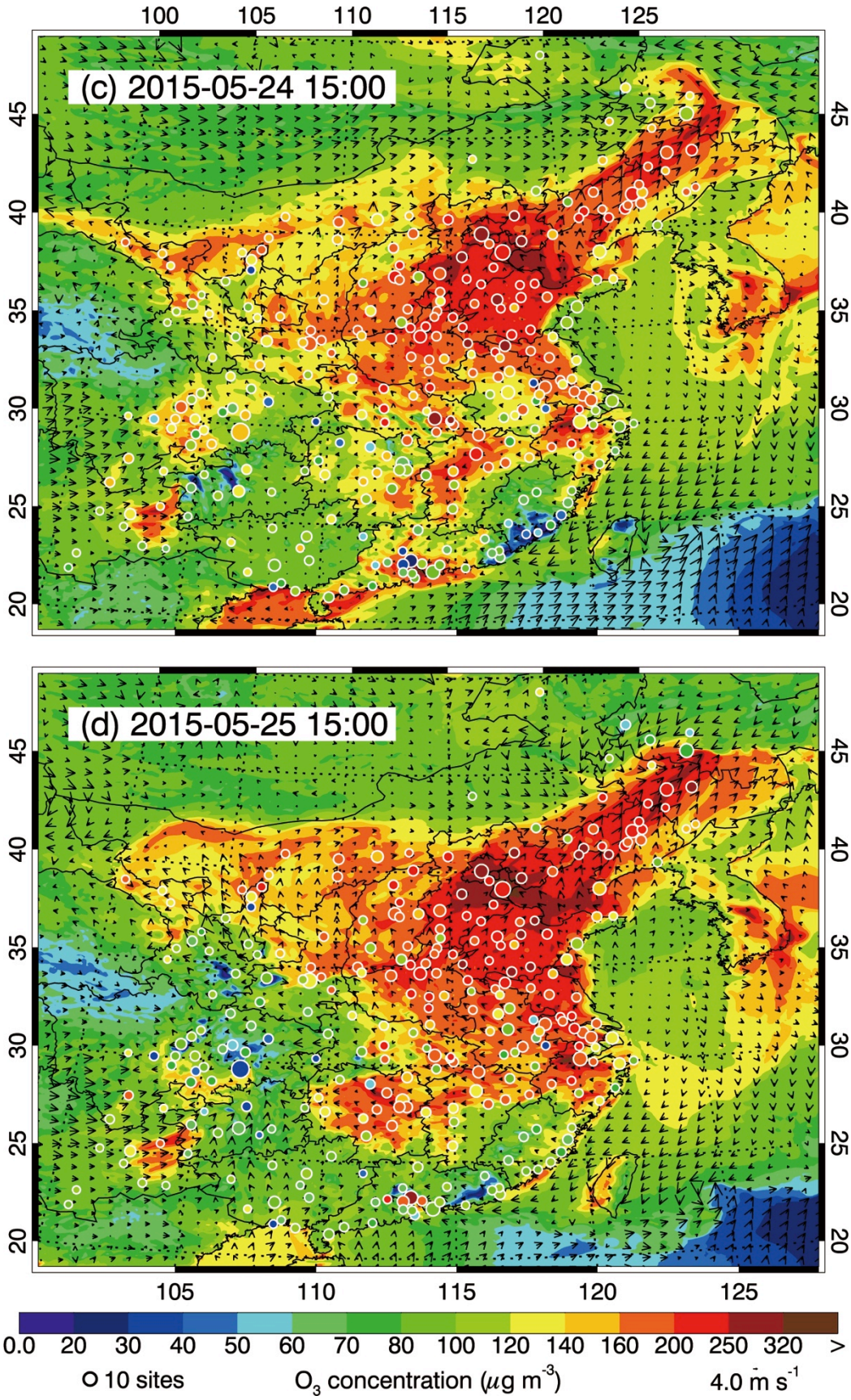

Figure 6 continued

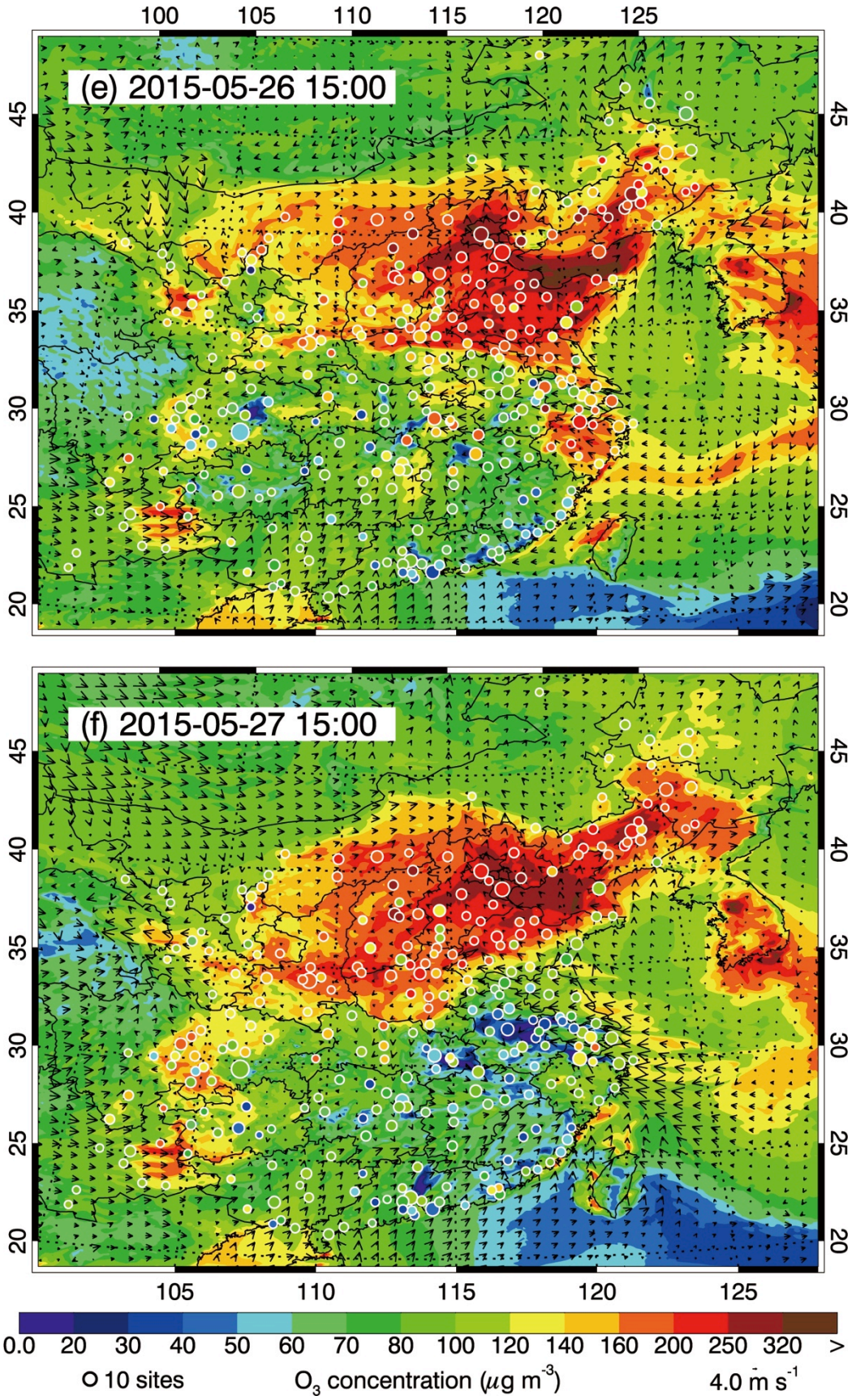

Figure 6 continued

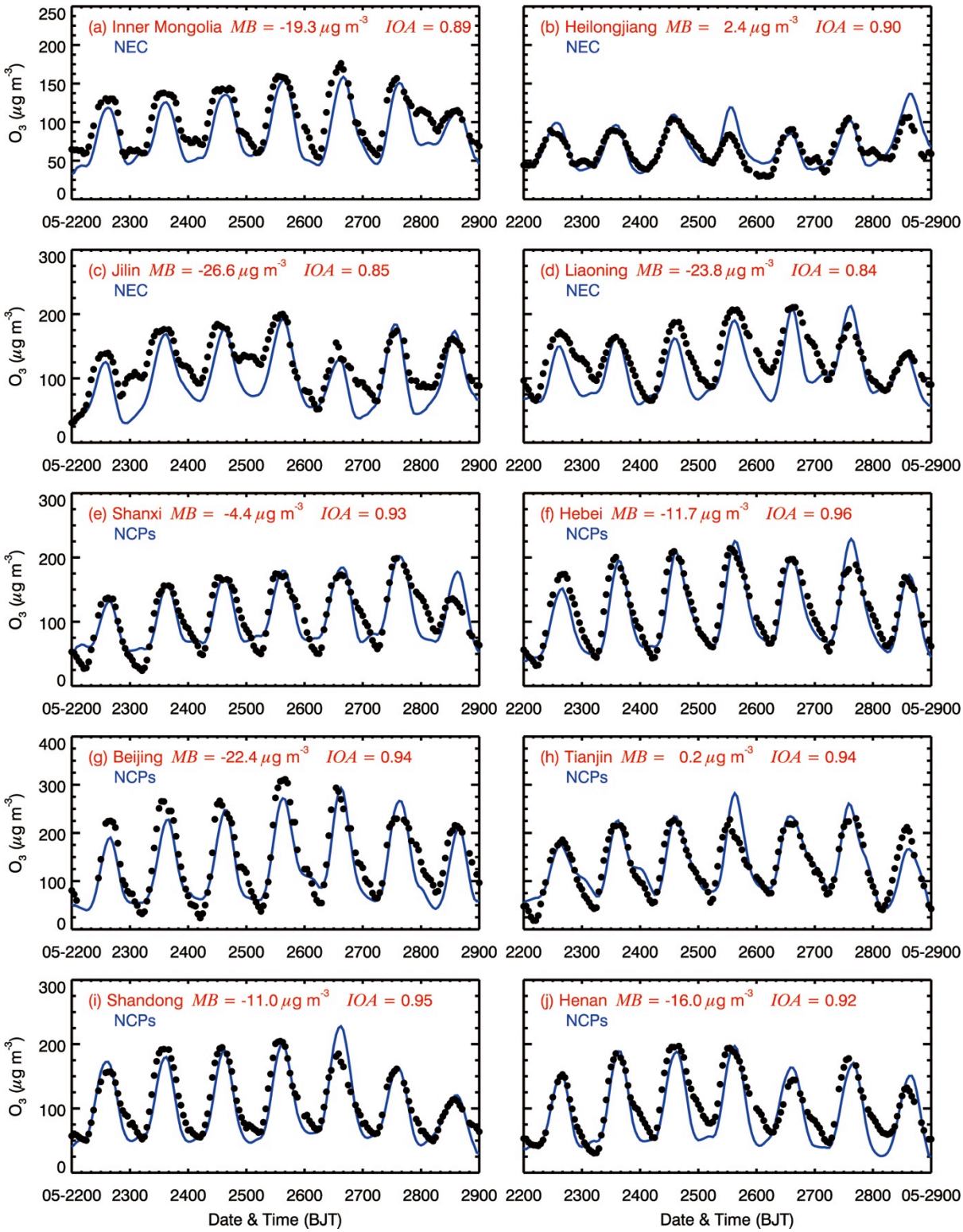

Figure 7 Comparison of measured (black dots) and predicted (blue line) diurnal profiles of near-surface O_3 averaged over all ambient monitoring stations in provinces of Eastern China from 22 to 28 May 2015.

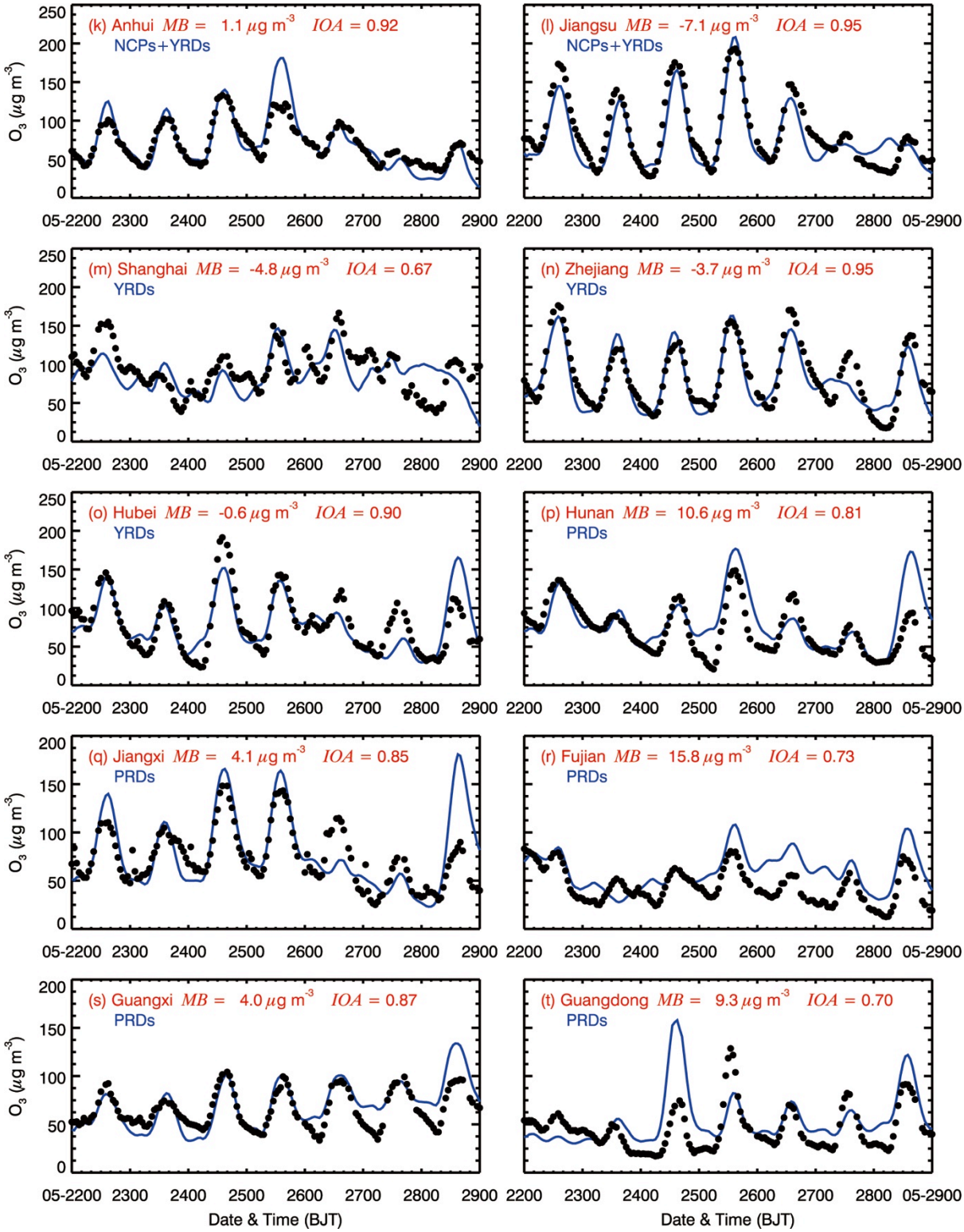

Figure 7 continued

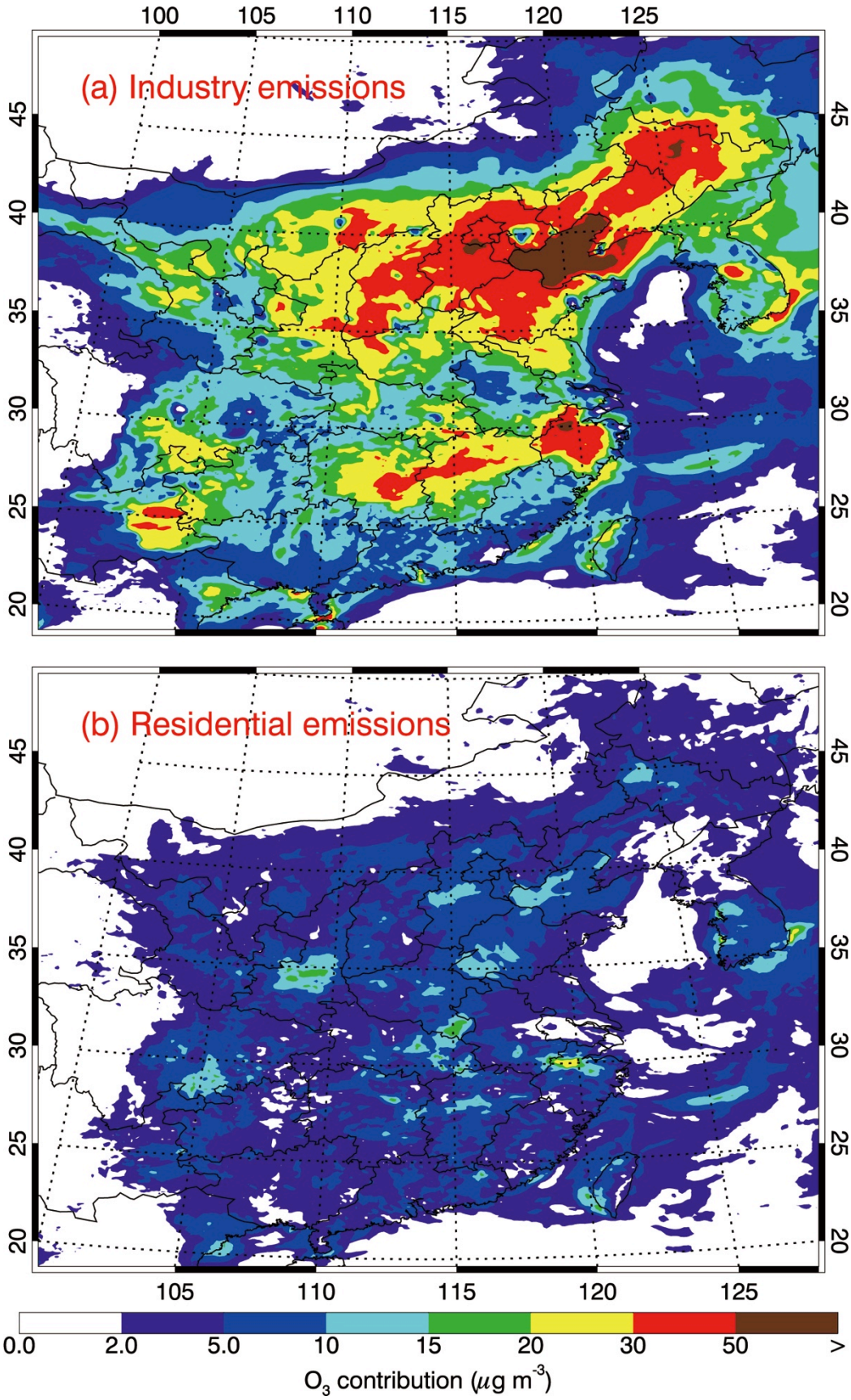

Figure 8 Distributions of the contribution to near-surface [O_3] averaged in the afternoon during the whole episode from (a) industry, (b) residential, (c) transportation, and (d) biogenic emissions.

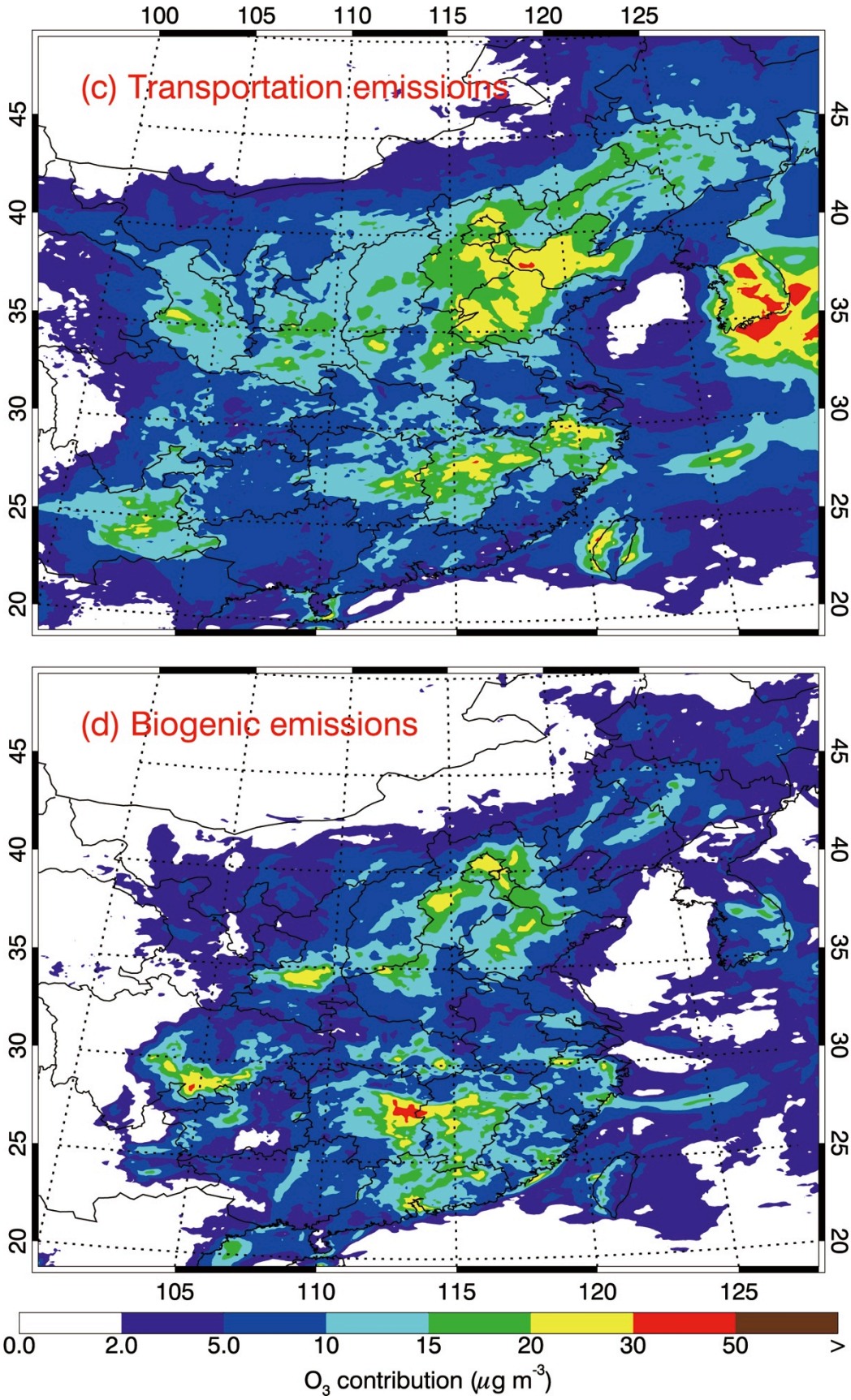

Figure 8 continued

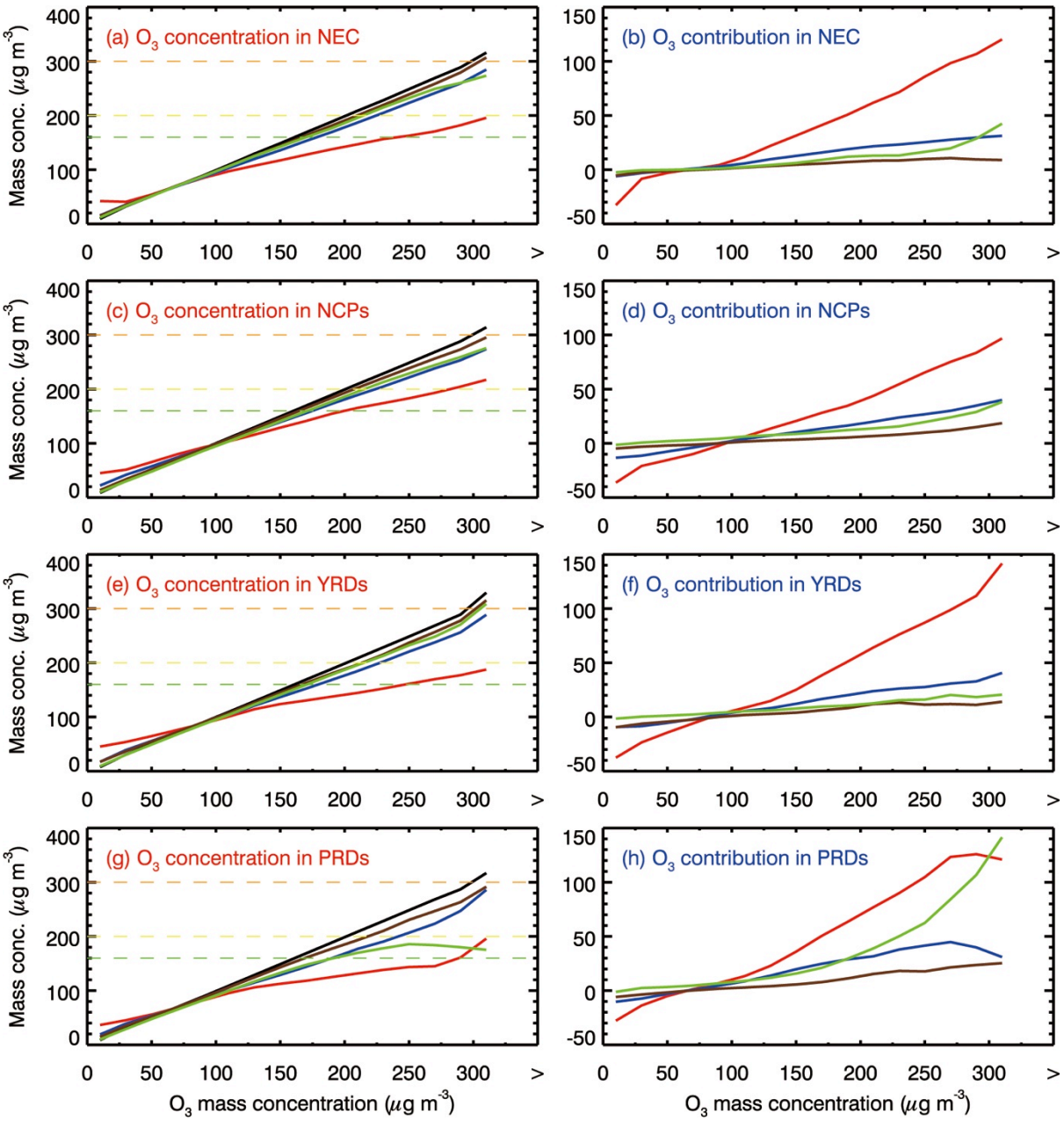

Figure 9 O_3 contributions of industry (red line), residential (brown line), transportation (blue line), and biogenic emissions (green line) in NEC, NCPs, YRDs, and PRDs, as a function of simulated [O_3] in the control case.

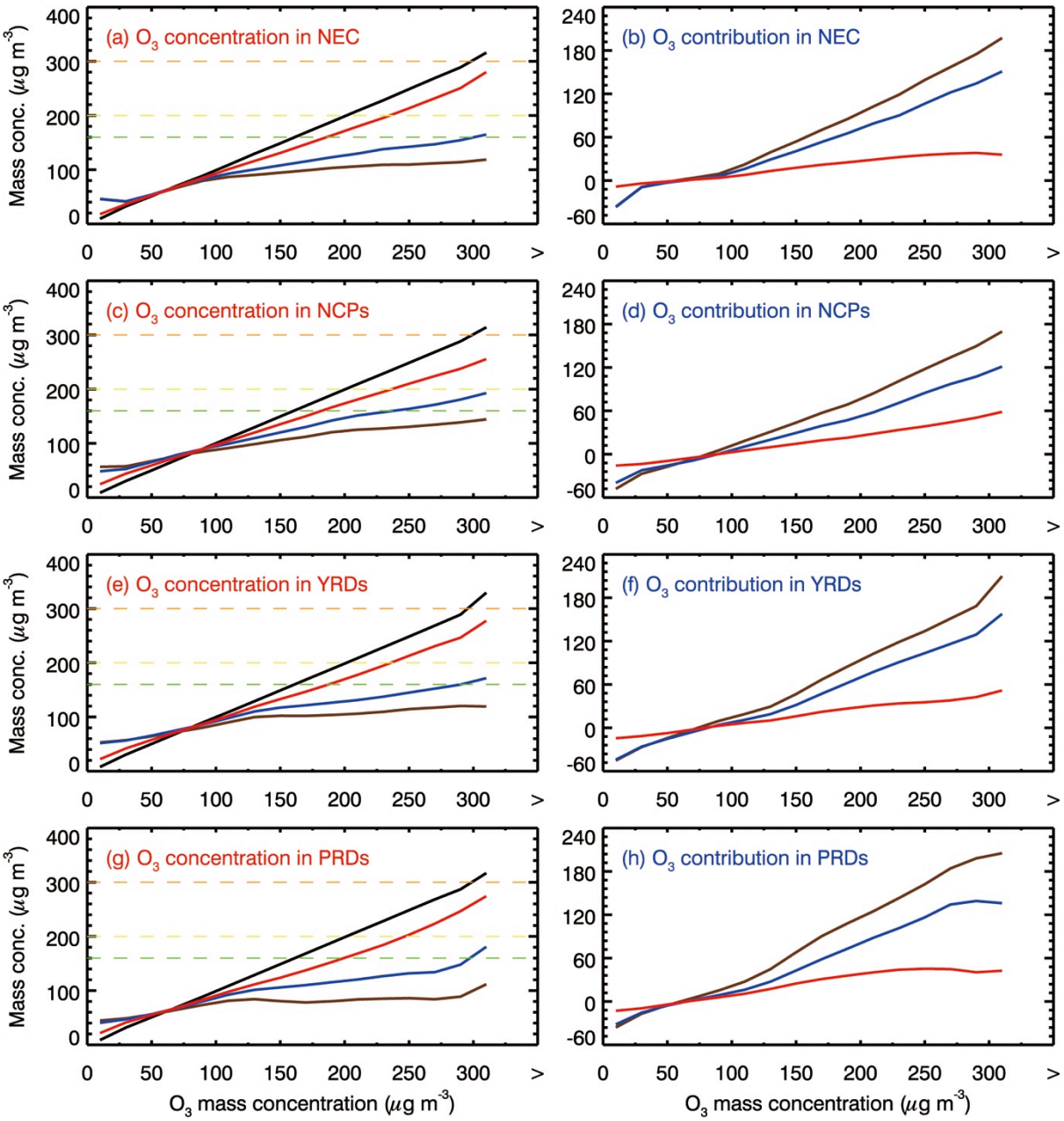

Figure 10 O_3 contributions of industry alone (red line), residential (brown line), and transportation emissions (blue line) in NEC, NCPs, YRDs, and PRDs, as a function of simulated [O_3] in the control case.

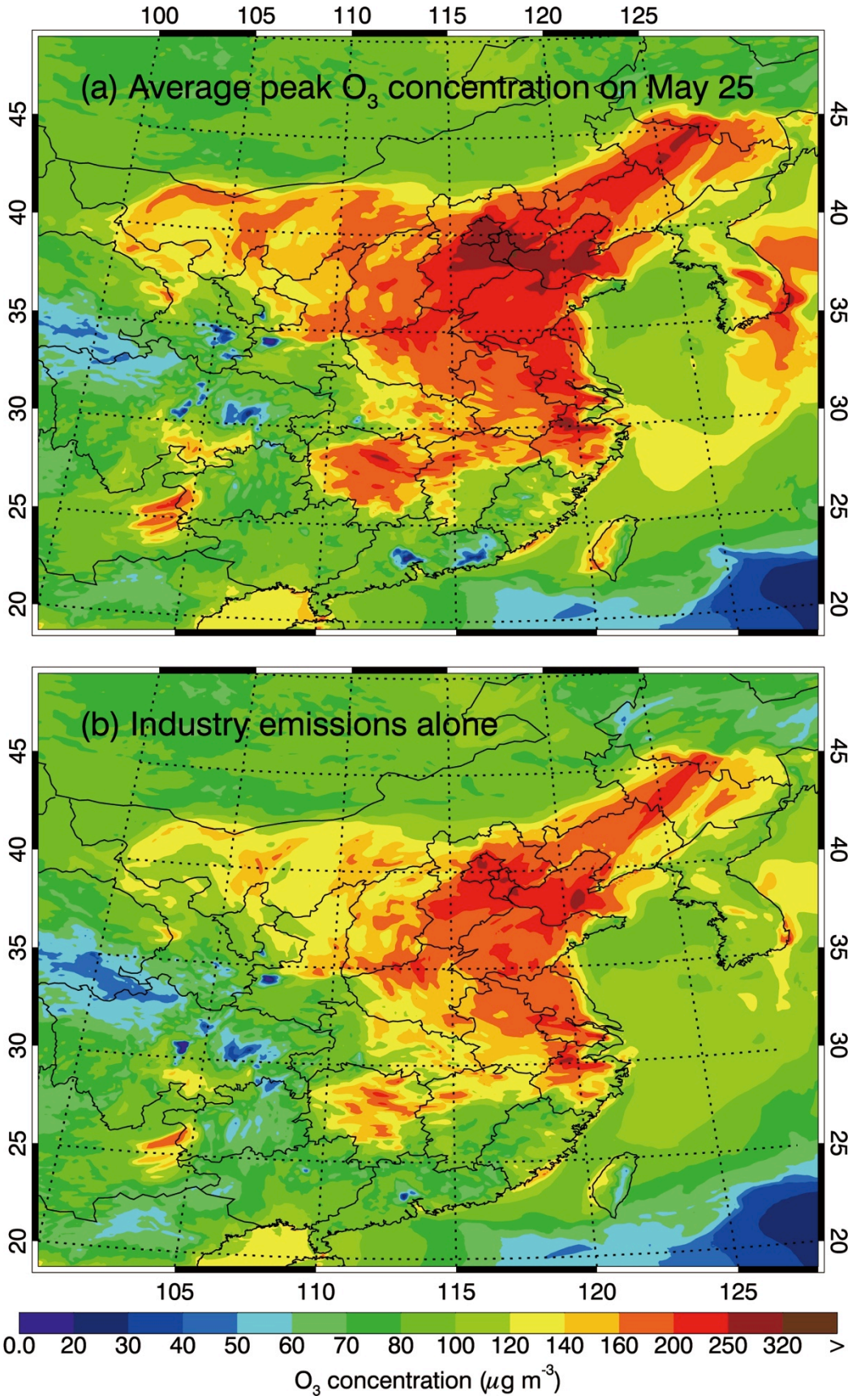

Figure 11 Distributions of the average O_3 concentration during peak time with (a) all anthropogenic emissions, (b) industry emissions alone, (c) residential emissions alone, and (d) transportation emissions alone on May 2015.

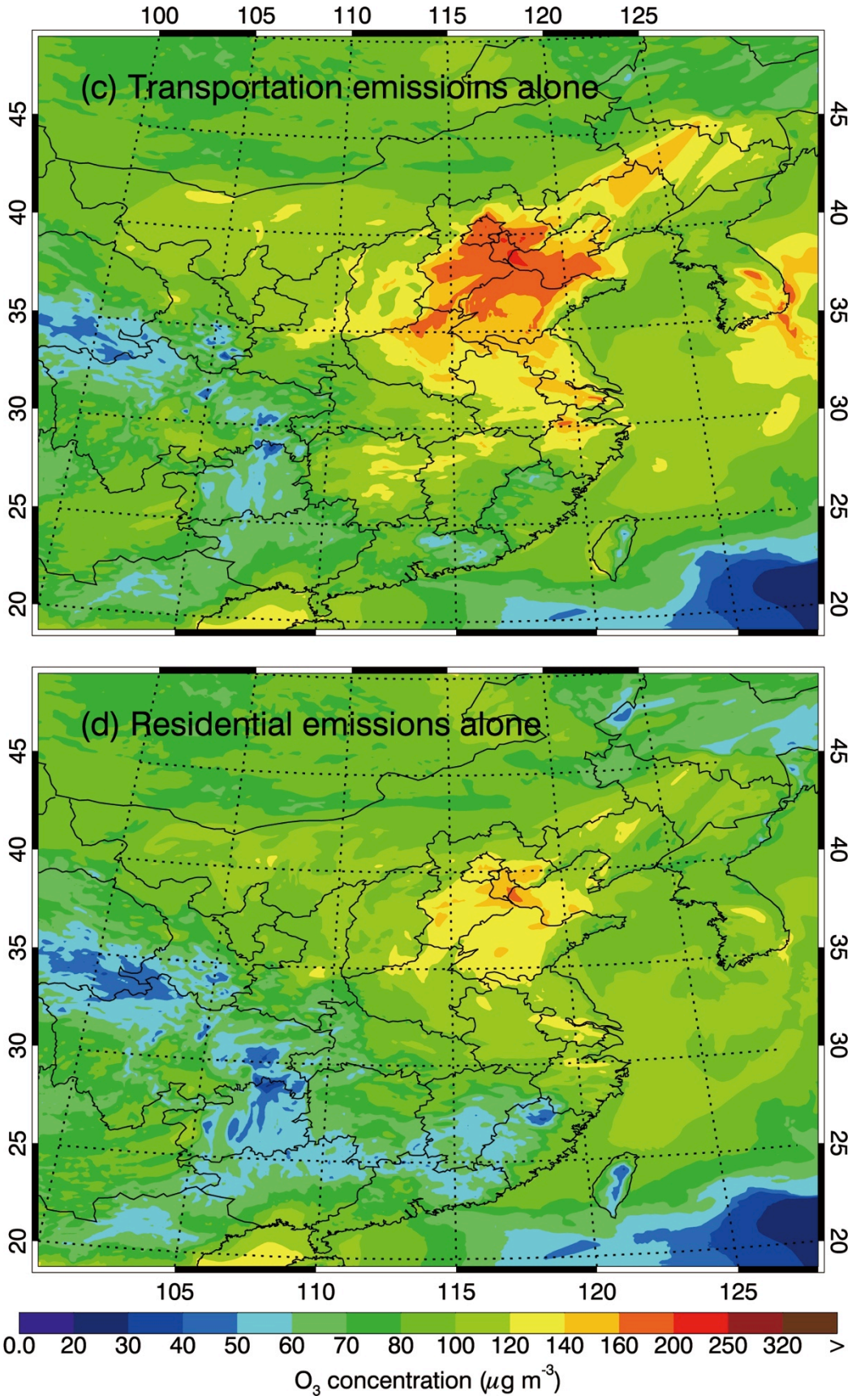

Figure 11 continued